

# Slow Light Augmented Unbalanced Interferometry for Extreme Enhancement in Sensitivity of Measuring Frequency Shift in a Laser

**Ruoxi Zhu<sup>1,\*</sup>, Zifan Zhou<sup>1</sup>, Jinyang Li<sup>2</sup>, Jason Bonacum<sup>3</sup>, David D. Smith<sup>4</sup>,  
and Selim M. Shahriar<sup>1,2,3</sup>**

<sup>1</sup>*Department of Electrical and Computer Engineering, Northwestern University, Evanston, IL 60208, USA*

<sup>2</sup>*Department of Physics and Astronomy, Northwestern University, Evanston, IL 60208, USA*

<sup>3</sup>*Digital Optics Technologies, Rolling Meadows, IL 60008, USA*

<sup>4</sup>*NASA Marshall Space Flight Center*

*\*Email: ruoxizhu2024@u.northwestern.edu*

## Abstract

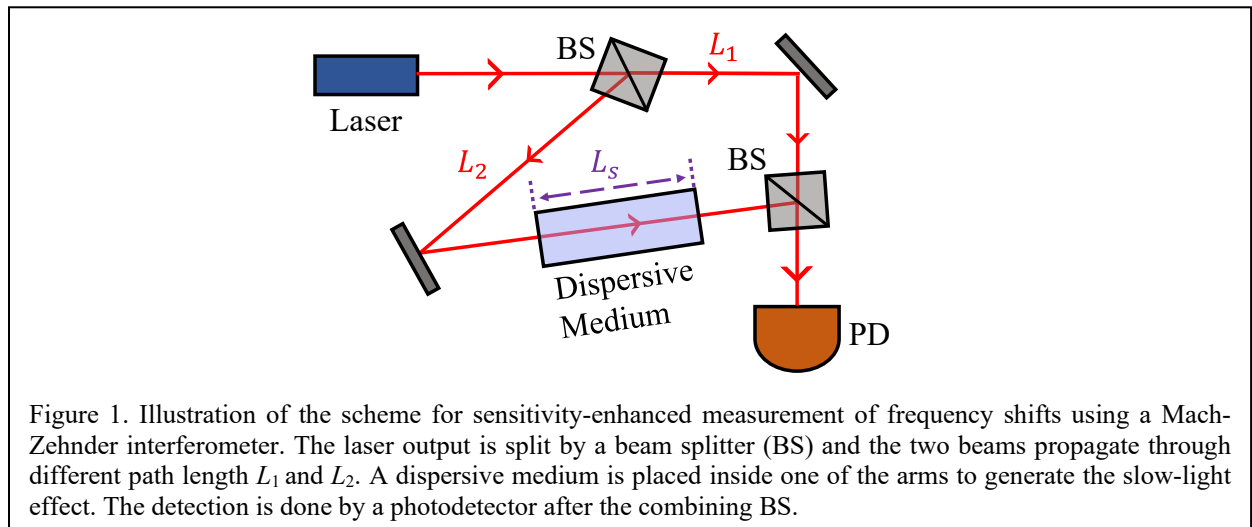
We demonstrate a slow-light augmented unbalanced Mach-Zehnder Interferometer (MZI) which can be used to enhance very significantly the sensitivity of measuring the frequency shift in a laser. The degree of enhancement depends on the group index of the slow-light medium, the degree of imbalance between the physical lengths of the two arms of the MZI, and the spectral width of the laser. For a laser based on a high-finesse cavity, yielding a narrow quantum noise limited spectral width, the group index has to be larger than the finesse in order to achieve enhancement in measurement sensitivity. For the reported results, strong slow-light effect is produced by employing electro-magnetically induced transparency via coherent population trapping in a buffer-gas loaded vapor cell of Rb atoms, with a maximum group index of  $\sim 1759$ . The observed enhancement in sensitivity for a range of group indices agrees well with the theoretical model. The maximum sensitivity enhancement factor realized is  $\sim 560$ ; much larger values can be obtained by using cold atoms for producing the slow-light effect. The sensitivity of any sensor that relies on measuring the frequency shift of a laser can be enhanced substantially using this technique. These include, but are not limited to, gyroscopes and accelerometers based on a conventional ring laser or a superluminal ring laser, and detectors for virialized ultra-light field dark matter.

## 1. Introduction

Many sensors rely on determining measurands based on shifts in frequencies of lasers. These include, but are not limited to, gyroscopes and accelerometers based on a conventional ring laser [1,2] or a superluminal ring laser [3], and detectors for virialized ultra-light field dark matter [4]. To achieve better precision in measuring frequency shifts, several schemes have been proposed employing superluminal lasers, which is a type of laser where the group velocity of light exceeds the speed of light in the vacuum [3,5,6,7,8,9, 10,11,12,13,14,15,16]. However, it is also possible to achieve a sensitivity enhancement with a slow-light augmented unbalanced Mach-Zehnder Interferometer (SLAUMZI). The idea is closely related to what Boyd et al. has shown, where the use of slow-light medium inside an unbalanced Mach-Zehnder Interferometer amplifies the number of fringes generated for a given change in the mean frequency [17]. However, their work did not take into account the spectral width of the laser, and how that affects the minimum measurable frequency shift (MMFS). Here, we determine the MMFS in a SLAUMZI, and how it depends on various parameters, including the finite linewidth of the laser and the degree of imbalance in the physical lengths of the two arms. Specifically, we identify the conditions under which the MMFS is smaller than what can be achieved using the technique of measuring the beat frequency between the test laser and a reference laser with a spectral width that is negligibly small compared to that of the test laser. We find that for many scenarios of practical interest, the reduction in the MMFS can be very large. Furthermore, we present experimental results demonstrating such an enhancement, in close agreement with the theoretical model. The rest of the paper is organized as follows. In Section 2, we present the theoretical model for enhancing sensitivity of measuring frequency shifts using a SLAUMZI. In Section 3, we present the experimental results for realizing a SLAUMZI and using it to demonstrate reduction in the MMFS. Concluding remarks are presented in Section 4.

## 2. Theory

The concept of slow-light augmented unbalanced interferometry (SLAUI) for the purpose of enhancing the sensitivity in measuring frequency shift can be realized using several different



configurations. These include, for example, a Mach-Zehnder Interferometer (MZI) or a Michelson Interferometer (MI) [18]. Consider first the case of an unbalanced MZI, as shown in Figure 1. Here, we denote the length of the upper arm as  $L_1$ , and the length of the lower arm as  $L_2$ , which can be expressed as  $L_2 = L_1 + L_0 + L_s$ , where  $L_s$  is the physical length of the slow-light medium and  $L_0$  is the intrinsic path-length difference (not shown explicitly in Figure 1). In what follows, we also assume the thickness of the windows of the glass cell to be negligible. We denote the frequency as  $\omega$ , and the refractive index experienced by the laser field in the slow-light medium as  $n(\omega)$ . The phase difference between the two paths can be expressed as:

$$\Phi(\omega) = L_0\omega/c_0 + n(\omega)L_s\omega/c_0, \quad (1)$$

where  $c_0$  is the vacuum speed of light. Therefore, the variation in the phase difference due to a change in the frequency can be expressed as:

$$\frac{d\Phi}{d\omega} = \frac{L_0}{c_0} + \frac{L_s}{c_0}n_g, \quad (2)$$

where  $n_g$  is the group index experienced by the laser at frequency  $\omega$ . We denote as the reference point the condition when the slow-light medium is replaced by vacuum, corresponding to unity group index (i.e.,  $n_g = 1$ ). In what follows, we will refer to the condition of  $n_g > 1$  as the slow-light case, and the condition of  $n_g = 1$  as the vacuum case. The fringe magnification factor, denoted as  $M$ , is then defined as the ratio between the phase difference variation in the slow-light case and the same for the vacuum case:

$$M \equiv \frac{(d\Phi/d\omega)_{SL}}{(d\Phi/d\omega)_{VAC}} = \frac{L_0/c_0 + n_g L_s/c_0}{L_0/c_0 + L_s/c_0} = \frac{\tau_0 + n_g \tau_D}{\tau_0 + \tau_D} \equiv \frac{\tau_{SL}}{\tau_{VAC}}, \quad (3)$$

where:

$$\tau_0 \equiv L_0/c_0; \quad \tau_D \equiv L_s/c_0; \quad \tau_{SL} \equiv \tau_0 + n_g \tau_D; \quad \tau_{VAC} \equiv \tau_0 + \tau_D. \quad (4)$$

When there is no slow-light effect, we get  $\tau_{SL} = \tau_{VAC}$  and  $M = 1$ .

We assume the signal at the detection port is maximum when the phase difference between the two arms has a null value, and denote it as  $S_0$ . The signal as a function of the phase difference then can be expressed as  $S_0 \cos^2[\Phi(\omega)/2]$ . We define as  $\omega_0$  the frequency at which the group index is evaluated, and denote as  $\Delta\omega$  the deviation away from this frequency (i.e.,  $\Delta\omega \equiv \omega - \omega_0$ ). The signal then can be expressed as:

$$\begin{aligned}
S &= S_0 \cos^2 \left( \left[ \Phi(\omega_0) + \frac{L_0}{c_0} \Delta\omega + \frac{L_s}{c_0} n_g \Delta\omega \right] / 2 \right) \\
&= S_0 \cos^2 \left( [\Phi(\omega_0) + \tau_0 \Delta\omega + \tau_D n_g \Delta\omega] / 2 \right) = S_0 \cos^2 ([\Phi(\omega_0) + \tau_{SL} \Delta\omega] / 2)
\end{aligned} \tag{5}$$

The findings of the analyses in the rest of the paper remain valid for an arbitrary value of the phase offset,  $\Phi(\omega_0)/2$ . As such, for notational clarity but without loss of generality, we set the value of  $\Phi(\omega_0)/2$  to zero, so that:

$$S = S_0 \cos^2(\tau_{SL} \Delta\omega / 2). \tag{6}$$

Equation (6) applies to the situation where the laser linewidth is assumed to be zero. Of course, in practice, the laser has a finite linewidth, greater than or equal to its quantum noise limited value known as the Schawlow-Townes Linewidth (STL). We consider first the limiting case where the linewidth equals the STL, which can be expressed as follows [19,20,21,22,2]:

$$\Gamma_{STL} = \frac{\hbar \omega \gamma_c^2}{2P_0} = \frac{\gamma_c^2}{2N} \equiv \frac{1}{\tau_{STL}}, \tag{7}$$

where  $P_0$  is the laser output power,  $\gamma_c$  is the cavity linewidth, given by the inverse of the cavity decay time,  $\tau_c$ , and  $N$  is the number of output photons per second. In this case,  $\tau_{STL}$  represents the coherence time,  $\tau_L$ , of the laser. The STL results from the loss of coherence due to spontaneous emission, and can be derived using many different ways, including the master equations approach, the Langevin noise operator approach, and the random walk approach [20,23], all yielding essentially the same result. Here, we consider the model employing the random walk approach, and limit our consideration to the case where the laser operates at the peak of the gain spectrum, so that the so-called Henry factor [20] can be ignored, noting that the analysis that follows can be easily extended to the more general case where the Henry factor is dominant. In this model, spontaneous emission events cause random phase jumps. The probability of such jumps is assumed to follow a Gaussian distribution.

To illustrate the effect of these phase jumps on the SLAUMZI signal, consider first the vacuum case corresponding to unity group index. We define as  $\tau_i$  the time for light to travel from the laser to the input port of the MZI, and  $\tau_1(\tau_2)$  as the time for light to travel along the upper (lower) arm of the MZI. Using the definitions summarized in Eqn. (4), we then get:

$$\begin{aligned}
\tau_1 &= L_1 / c_0 \\
\tau_2 &= L_2 / c_0 = \tau_1 + \tau_0 + \tau_D = \tau_1 + \tau_{VAC}
\end{aligned} \tag{8}$$

Thus, at the output port of the SLAUMZI, the field arriving via the upper arm at time  $t$  is shifted in phase by the phase-jump,  $\phi$ , that occurred at a time  $t - (\tau_i + \tau_1)$ . On the other hand, the

field arriving via the lower arm at time  $t$  is shifted in phase by the phase-jump,  $\phi_2$ , that occurred at a time  $t - (\tau_1 + \tau_2)$ . Therefore, the unity-group-index SLAUMZI signal can be expressed as:

$$\begin{aligned} S &= S_0 \cos^2 [(\tau_{VAC} \Delta\omega + \phi_2 - \phi_1) / 2] \\ &= \frac{S_0}{2} + \frac{S_0}{2} [\cos(\tau_{VAC} \Delta\omega) \cos(\Delta\phi) - \sin(\tau_{VAC} \Delta\omega) \sin(\Delta\phi)] \end{aligned} \quad (9)$$

where  $\Delta\phi = \phi_2 - \phi_1$ . Thus, the two instances when the laser phase jumps to  $\phi_1$  and  $\phi_2$  are separated by the time difference  $\tau_{VAC} = \tau_2 - \tau_1$ .

Consider next the slow-light case, corresponding to the non-unity group index. We define  $\tilde{\tau}_1$  ( $\tilde{\tau}_2$ ) as the time for light to travel along the upper (lower) arm of the MZI:

$$\begin{aligned} \tilde{\tau}_1 &= L_1 / c_0 = \tau_1 \\ \tilde{\tau}_2 &= \tilde{\tau}_1 + \tau_0 + nL_s / c_0 = \tilde{\tau}_1 + \tau_0 + n\tau_D = \tilde{\tau}_1 + \tau_{ND} \end{aligned} \quad (10)$$

where  $n$  is the phase index (*not* the group index) of the slow-light medium, and we have defined  $\tau_{ND} \equiv \tau_0 + n\tau_D$ . Since the experiment is to be carried out for a continuous wave (CW) laser, it is proper to use the phase index for the propagation of the mean field. If the spectral width of the laser is due strictly to the STL caused by spontaneous emission, the phase jumps can be modeled as occurring instantaneously (according to the Markov approximation used in modeling the coupling between the atoms and the bath of vacuum modes). On the other hand, the bandwidth of the positive dispersion that causes the slow-light effect is typically very small (of the order of a few MHz in the experiment reported here). As such, it is a good approximation to assume that the phase jump would also propagate through the slow-light medium at essentially the phase velocity, and not the group velocity. Without loss of generality, we see that  $\tilde{\tau}_2 = \tilde{\tau}_1 + \tau_{ND} = \tau_2$ , and  $\tilde{\tau}_2 - \tilde{\tau}_1 = \tau_2 - \tau_1 = \tau_{ND}$ . As such, the non-unity group index SLAUMZI signal can be expressed as:

$$\begin{aligned} S &= S_0 \cos^2 [(\tau_{SL} \Delta\omega + \phi_2 - \phi_1) / 2] \\ &= \frac{S_0}{2} + \frac{S_0}{2} [\cos(\tau_{SL} \Delta\omega) \cos(\Delta\phi) - \sin(\tau_{SL} \Delta\omega) \sin(\Delta\phi)] \end{aligned} \quad (11)$$

where  $\Delta\phi = \phi_2 - \phi_1$ , and the two instances when the laser phase jumps to  $\phi_1$  and  $\phi_2$  are separated by the time difference  $\tau_{ND} = \tilde{\tau}_2 - \tilde{\tau}_1 = \tau_2 - \tau_1$ . It should be noted that in this case the time parameter that determines the scale of the signal fringes is now  $\tau_{SL} \equiv \tau_0 + n_g \tau_D$ , which is much larger than  $\tau_{ND} = \tau_0 + n\tau_D$  when the group index is substantially larger than unity, since the phase index is very close to unity if diluted vapor gas at close to room temperature or cold atoms are used for generating the slow-light effect.

The probability of having two instances of phase jumps separated by  $\tau_{ND}$  can be expressed as [23]:

$$f(\Delta\phi_{\tau_{ND}}) = \frac{1}{\sqrt{2\pi\tau_{ND}/\tau_{STL}}} \exp\left(-\frac{\Delta\phi_{\tau_{ND}}^2}{2(\tau_{ND}/\tau_{STL})}\right). \quad (12)$$

Therefore, the output power can be expressed as:

$$S = \frac{S_0}{2} + \frac{S_0}{2} \left[ \cos(\tau_{SL}\Delta\omega) \langle \cos(\Delta\phi_{\tau_{ND}}) \rangle - \sin(\tau_{SL}\Delta\omega) \langle \sin(\Delta\phi_{\tau_{ND}}) \rangle \right]. \quad (13)$$

The expectation value  $\langle \cos(\Delta\phi_{\tau_{ND}}) \rangle$  can be calculated as:

$$\int_{-\infty}^{+\infty} \cos(\Delta\phi_{\tau_{ND}}) f(\Delta\phi_{\tau_{ND}}) d(\Delta\phi_{\tau_{ND}}) = \exp\left(-\frac{\tau_{ND}}{2\tau_{STL}}\right). \quad (14)$$

It is obvious that  $\langle \sin(\Delta\phi_{\tau_{ND}}) \rangle = 0$  because of the symmetry around the origin. Therefore, the output power can be expressed as:

$$S = \frac{S_0}{2} + \frac{S_0}{2} \exp\left(-\frac{\tau_{ND}}{2\tau_{STL}}\right) \cos(\tau_{SL}\Delta\omega). \quad (15)$$

Thus, the contrast is decreased as the length imbalance increases, which is consistent with the result that interference signal disappears when the time delay greatly exceeds the coherence time. For the case where no slow light is used, the expression for the signal becomes:

$$S = \frac{S_0}{2} + \frac{S_0}{2} \exp\left(-\frac{\tau_{ND}}{2\tau_{STL}}\right) \cos(\tau_{ND}\Delta\omega). \quad (16)$$

For the vacuum case, we have  $n = 1$ , which means  $\tau_{ND} = \tau_{VAC}$ , and the corresponding expression for the signal is:

$$S = \frac{S_0}{2} + \frac{S_0}{2} \exp\left(-\frac{\tau_{VAC}}{2\tau_{STL}}\right) \cos(\tau_{VAC}\Delta\omega) \quad (17)$$

It should be noted that this expression for the signal for a conventional unbalanced MZI (UMZI) is well accepted. For example, the approach used in Ref. [24] for deriving the spectral width of a Fabry-Perot cavity can be easily adopted to get this expression for the UMZI.

For potential applications, it is important to determine the minimum measurable frequency shift (MMFS) in the SLAUMZI and compare it with the MMFS for the conventional approach [2,25], which is limited by the laser linewidth and the measurement time. The MMFS for the SLAUMZI is given by the uncertainty in the observed value of the laser frequency, expressed as:

$$\delta\omega_{SLAUMZI} = \left| \frac{\Delta S}{\partial S / \partial \omega} \right|. \quad (18)$$

where  $\Delta S$  is the standard deviation of the signal, accounting for all sources of noise. In what follows, we denote  $N$  as the number of photons per second received by a photodetector corresponding to the peak signal  $S_0$ , and  $\tau_M$  as the measurement time. We assume that the value of  $L_0 + L_s$  in the SLAUMZI is restricted to be less than a meter, so that the value of  $\tau_{VAC}$  is less than 3.3 nsec. To estimate a typical value of  $\tau_{STL}$ , we consider a 70 cm long, three-mirror ring laser with two perfect reflectors, an output coupler with an intensity reflectivity of 0.5, and an output power of 40 mW, which does not experience additional broadening due to the Henry factor[20]. For these parameters, the value of the STL is  $\sim 5.6$  mHz [26]. If the laser is shorter by a factor of  $10^3$ , which would be typical for a diode laser, the value of STL would be larger by a factor of  $10^6$ , yielding a value of 5.6 kHz. The Henry factor, which is highly relevant for a diode laser, is typically of the order of 50 [20], which would make the value of STL to be  $\sim 280$  kHz (which is close to the value of the measured linewidth of the laser we have used as the source for the SLAUMZI). The value of  $\tau_{STL}$  for such a laser would be  $\sim 3.6 \mu\text{sec}$ . As such, it is reasonable to make the approximation that  $\tau_{VAC} \ll \tau_{STL}$ .

The ideal method for measuring any shift in the frequency of the laser would make use of the so-called hopping process [27], which would work as follows for the SLAUMZI. The frequency of the laser would be modulated with a square wave, thus making it jump by a value of  $\Delta\omega = \pm[\pi / (2\tau_{SL})]$ , and the signal observed at these two extrema (corresponding to maximum slopes) would be subtracted from one another. If the unmodulated value of the laser frequency corresponds to the peak of the signal, for example, then the subtracted signal would be zero, in the absence of any noise. Any deviation of the subtracted signal away from zero would then represent a shift in the laser frequency. It can be shown that the minimum frequency uncertainty obtained using this hopping method is the same as what one would obtain if the signal is measured at the point where it has the highest slope [27]. As such, in what follows, we determine the value of  $\delta\omega_{SLAUMZI}$  at one of these points, corresponding to a bias frequency shift of  $\Delta\omega = \pi / (2\tau_{SL})$ .

We consider first the case where the experiment is limited by quantum noise only. In that case, the variance of the signal is due simply to the shot noise, which dictates that the uncertainty in the number of photons detected equals the square-root thereof. Assuming ideal detection efficiency, we then get that for a bias frequency shift of  $\Delta\omega = \pi / (2\tau_{SL})$  the minimum uncertainty in the laser frequency is then given by:

$$\delta\omega_{SLAUMZI} = \frac{\sqrt{N\tau_M / 2}}{(N\tau_M / 2)\tau_{SL} \exp[-\tau_{VAC} / (2\tau_{STL})]}. \quad (19)$$

Since  $\tau_{VAC} \ll \tau_{STL}$ , this equation simplifies to:

$$\delta\omega_{SLAUMZI} \approx \frac{\sqrt{2}}{\tau_{SL}[1 - \tau_{VAC} / (2\tau_{STL})]\sqrt{N\tau_M}} \approx \frac{\sqrt{2}}{\tau_{SL}\sqrt{N\tau_M}}. \quad (20)$$

If we denote by  $\eta$  the quantum efficiency of the detector, and by  $\sigma$  the attenuation of the signal [28,29,30], then the equation becomes:

$$\delta\omega_{SLAUMZI} \approx \frac{\sqrt{2}}{\tau_{SL}\sqrt{\eta\sigma N\tau_M}} \quad (21)$$

To compare this sensitivity with what can be achieved using the conventional approach, we consider the standard technique whereby the frequency of the laser is measured by beating it with a reference laser which has a much narrower STL (delta function limit). A closely related technique is used, for example, in a He-Ne ring laser gyroscope [2,25]. In that case, the laser in one direction beats with the laser in the other direction. Assuming full suppression of common mode noise, the observed uncertainty is then the sum of the uncertainties in the frequency of the laser in each direction, which in turn determines the uncertainty in the measured rotation rate. Under quantum noise limited operation, it can be shown [2] that the spectral uncertainty in such a measurement is given by the geometric mean of the sum of the STLs of each laser and the measurement bandwidth. The derivation of this result is summarized in Section 1.2 in **Supplement I**. In the case we are considering, where the STL of the reference laser is vanishingly small, it would then follow that the spectral uncertainty in the measurement of the test laser is given by the geometric mean of the STL of the test laser and the measurement bandwidth. Assuming the same values of  $\tau_M$  and  $N$  and using the notation introduced above, for ideal quantum efficiency, we can write the MMFS for the standard technique as:

$$\delta\omega_{STD} = \sqrt{\frac{\gamma_{STL}}{\tau_M}} = \sqrt{\frac{\gamma_c^2}{2N\tau_M}} = \frac{1}{\tau_c\sqrt{2N\tau_M}}. \quad (22)$$

In Ref. [21], it has been shown that this expression for the MMFS for a quantum noise limited laser can be derived without specifying a particular approach (such as the beating of two lasers) for the measurement process. The derivation of this result is summarized in Section 1.1 of **Supplement I**. However, this expression must satisfy the fundamental uncertainty relation between the spectral uncertainty and the measurement time:  $\delta\omega \geq 1/\tau_m$ . Thus, in order for the expression for the MMFS shown in Eqn. (22) and derived in Ref. [21] to remain valid, the measurement time must satisfy the fundamental Heisenberg uncertainty limit:

$$\delta\omega \cdot \delta t \geq 1. \quad (23)$$

Since  $\delta t = \tau_M$ , this implies the following constraint:

$$\tau_M \geq 2N\tau_c^2. \quad (24)$$

In Section 2 of **Supplement I**, we have shown typical values of an ideal, quantum noise limited He-Ne ring, with the STL given by Eqn. (7). Specifically, we show that even for a modest set of parameters, we can find a condition (see the 4<sup>th</sup> row of Table 1 in **Supplement I**) under which  $N$  is  $\sim 3.2 \cdot 10^{16} \text{ sec}^{-1}$  and  $\tau_c$  is  $\sim 0.3 \cdot 10^{-6}$ , so that  $2N\tau_c^2$  is  $\sim 1.8 \cdot 10^{10}$ . This would correspond to a



constraint that  $\tau_M \geq 1.8 \cdot 10^{10} \tau_c$ . However, the derivation of Eqn. (22) in Ref. [21] only assumes that  $\tau_M \geq \tau_c$ . Thus, if Eqn. (22) were to hold as long as  $\tau_M \geq \tau_c$ , this example would allow one to violate the fundamental uncertainty limit. As such, it must be concluded that Eqn. (22) is not a fundamental limit for the MMFS.

We consider now a specific measurement scheme, *without using slow-light*, that can easily violate the limit shown in Eqn. (22). Specifically, we consider the use of an ideal, unbalanced MZI, for which the signal is given by Eqn. (17). In such a scenario, the MMFS would diverge in two limits: for  $\tau_{VAC} = 0$  (corresponding to no imbalance) and  $\tau_{VAC} \gg 2\tau_{STL}$  (corresponding to a time lag between the two arms that far exceeds the coherence time of the laser). As shown in Section 2 of **Supplement I**, the optimal sensitivity is obtained when  $\tau_{VAC} = 2\tau_{STL}$ . For this condition, we find the MMFS to be:

$$\delta\omega_{UMZI} = \frac{e}{\sqrt{2S_0}\tau_{STL}} \quad (25)$$

We also show that for this sensitivity:

$$\frac{\delta\omega_{UMZI}}{\delta\omega_{STD}} = \frac{e}{\sqrt{2S_0}\tau_{STL}} \cdot \left( \sqrt{\frac{\hbar\omega}{2P_{out}\tau_c^2\tau_M}} \right)^{-1} = e \frac{\tau_c}{\tau_{STL}} \quad (26)$$

This quantity can easily be much less than unity. For example, if we again consider the case shown in row 4 of Table 1 in Supplement I, we have  $\tau_c \approx 0.3 \cdot 10^{-6}$  seconds, and  $\tau_{STL} \approx 5.1 \cdot 10^3$  seconds, so that the ratio in Eqn. (26) becomes  $\sim 1.6 \cdot 10^{-10}$ . Thus, even a simple unbalanced MZI can produce an improvement in the MMFS by a factor of  $\sim 6$  billion. Of course, in order to accommodate the length imbalance corresponding to  $\tau_c = 2\tau_{STL}$  the physical length of such an MZI would be  $\sim 3 \cdot 10^{12}$  meters, which is absurdly large. Nonetheless, this example shows clearly that the MMFS for the standard technique, as expressed in Eqn. (22), is not a fundamental limit. What we show in this paper is a technique for realizing this inherent advantage of using an UMZI for detecting frequency shifts, without using an absurdly large imbalance in the physical lengths of the two arms.

To determine the ratio between the MMFS's of the SLAUMZI and that of the standard technique, we first modify the expression for the latter by taking into account the effect of sub-unity quantum efficiency,  $\eta$ , of the detector:

$$\delta\omega_{STD} = \frac{1}{\tau_c \sqrt{2\eta N \tau_M}}. \quad (27)$$

Comparing Eqn. (27) with Eqn. (21), we thus get:

$$\frac{\delta\omega_{SLAUMZI}}{\delta\omega_{STD}} \approx \frac{2\tau_c}{\sqrt{\sigma}\tau_{SL}} \quad (28)$$

Eqn. (28) can be expressed in terms of the length scales as:

$$\frac{\delta\omega_{SLAUMZI}}{\delta\omega_{STD}} \approx \frac{2F\tau_{RT}}{(\tau_0 + n_g\tau_D)\sqrt{\sigma}} = \frac{2FL_c}{(L_0 + n_gL_D)\sqrt{\sigma}}, \quad (29)$$

where  $F$  is the cavity finesse and  $L_c = c_0\tau_{RT}$  is the cavity length for the laser. In the limit where  $n_gL_D \gg L_0$  and the cavity length equals the length of the dispersive media, we can approximate the ratio to:

$$\frac{\delta\omega_{SLAUMZI}}{\delta\omega_{STD}} \sim \frac{2F}{n_g\sqrt{\sigma}}. \quad (30)$$

Thus, in order to achieve a smaller MMFS than what can be obtained with the conventional technique, the group index in an SLAUMZI must be larger than 2 times the finesse of the laser, in the ideal limit of  $\sigma \rightarrow 1$ .

The results we have presented above show that, for proper choice of parameters, the SLAUMZI may be used to enhance the sensitivity of any sensor where the measurand of interest is proportional to the shift in the frequency of a laser. One device that falls in this category is an active ring laser gyroscope. We consider first the case where the rotation rate is inferred simply from the shift in the frequency of a unidirectional ring laser. The approach for determining the rate of rotation via measurements of shifts in the frequencies of two counter-propagating lasers is discussed later. One issue of concern for rotation sensing using this approach is that the SLAUMZI itself experiences the Sagnac effect in the phase difference between two arms. This problem can be overcome by making use of a “figure 8” type configuration for the SLAUMZI, so that the net enclosed area is zero. In this context, it is important to note that the improvement in MMFS using a slow-light medium with a group index greater than unity can be realized even without a difference in the physical lengths of the two arms of the MZI. Alternatively, one can use a slow-light augmented unbalanced Michelson Interferometer (SLAUMI). However, since each of the SLAUMI would have standing waves, it would be very difficult to realize efficient slow-light effect in one arm using the technique of coherent population trapping. We note that it is also possible to realize a slow-light enhanced Fabry-Perot ring resonator (in a figure-8 configuration for rotation sensing) for which one must take into account effects of multiple interference among the laser beams generated during multiple bounces off the mirrors [25]. The analysis for such a case is more involved, without a simple analytic expression for the enhancement in the MMFS, and will be presented in a future paper.

In a typical He-Ne Ring Laser Gyro, the finesse is on the order of  $10^4$ . Thus, a slow light with a group index of  $10^7$ , for example, would increase the measurement accuracy for rotating sensing by nearly three orders of magnitude, according to Eqn. (30). Of course, if a superluminal laser is used for rotation sensing, this enhancement would be above the factor of enhancement achievable

using the superluminal laser alone, assuming that the STL of a superluminal laser remains essentially the same as that of a conventional laser with identical operating parameters, such as the cavity length, cavity finesse, and the output power [6].

It is noteworthy that even though the analysis of the MMFS is conducted by assuming the laser linewidth is quantum noise limited, there is no fundamental requirement for making such an assumption. In fact, for any laser that has a finite linewidth  $\Gamma_L$ , we can define the following quantity:

$$\tau_L \equiv \frac{1}{\Gamma_L}. \quad (31)$$

The behavior of such a laser can also be modeled as originating from random phase jumps. Here, for simplicity, we assume the phase jumps will have a Gaussian probability distribution (in general, it would be necessary to characterize the noise processes carefully to determine the nature of the probability distribution.) As such, the steps shown in eqns. (9) through (15) would apply in this case. For such a laser, the MMFS for the standard technique can be expressed simply as:

$$\delta\omega_{STD} = \frac{1}{\sqrt{\eta\tau_L\tau_M}}. \quad (32)$$

Therefore, with such a laser, the ratio between the MMFS for the SLAUMZI and the standard technique, which represents the Sensitivity Enhancement Factor (SEF), to be denoted as  $R$ , becomes:

$$R \equiv \frac{\delta\omega_{SLAUMZI}}{\delta\omega_{STD}} = \frac{\sqrt{2} / (\tau_{SL} \sqrt{\sigma\eta N \tau_M})}{1 / \sqrt{\eta\tau_L\tau_M}} = \frac{1}{\tau_{SL}} \sqrt{\frac{2\tau_L}{\sigma N}}. \quad (33)$$

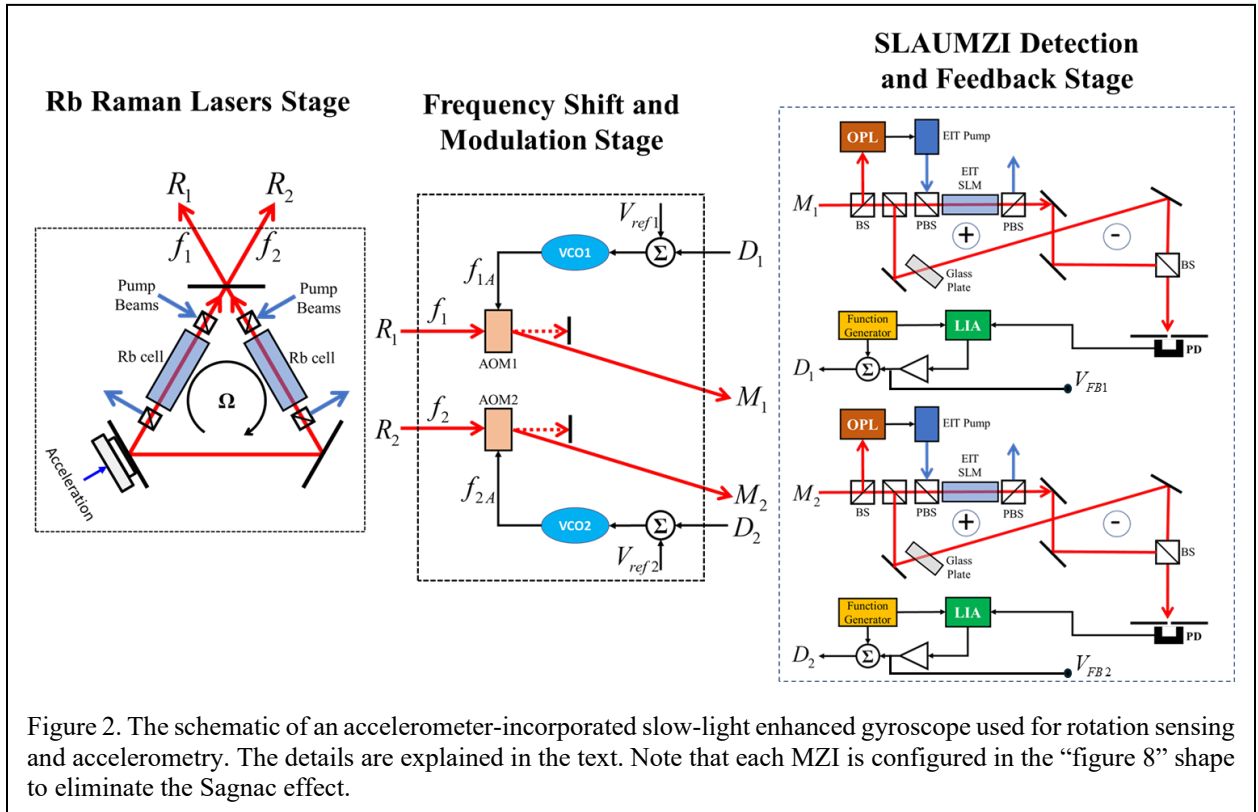
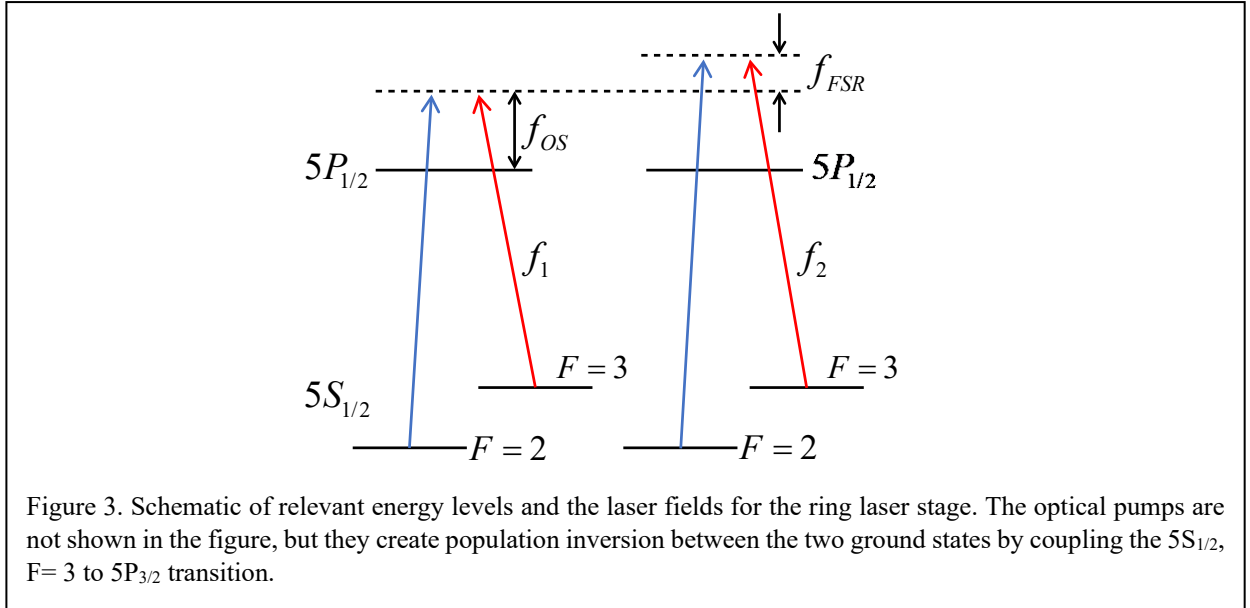


Fig.2 shows a configuration for a SLAUMZI enhanced gyroscope and accelerometer. The left panel shows a pair of bi-directional Raman lasers, which can be either subluminal [26] or superluminal [14], employing gain from two separate cells, without any cross-talks. In order to take advantage of the SLAUMZI technique, it is necessary to employ a slow-light medium with a very large group index. One approach for achieving a group index as large as ten million is to make use of the process of electromagnetically induced transparency (EIT) in a  $\Lambda$  system [31,32]. For such a process, both legs of the beams have to be resonant with respect to the intermediate state. On the other hand, a Raman laser is always detuned by nearly a GHz away from any excited state. As such, in order to realize the EIT process, it is necessary to shift the Raman laser output with an acousto-optic modulator (AOM), for example, so that the shifted beam becomes resonant with one leg of the  $\Lambda$  system. In addition, it is necessary to ensure that the optical fields are phase coherent, even though they would differ in frequency by the ground state splitting. To fulfill this requirement, it is necessary to make use of another laser for the second leg, and off-set phase lock it to the Raman laser.

There are two laser outputs  $R_1$  and  $R_2$  through the output coupler. Assume the lasing frequencies of these two laser outputs are  $f_1$  and  $f_2$ , respectively. Consider first one of the outputs, for example,  $R_1$ . This is passed through an acoustic optical modulator (AOM) to produce  $M_1$  with a frequency shift, which is denoted as  $f_{1A}$  and is determined by the voltage reference  $V_{ref1}$  in the voltage controlled oscillator (VCO). The  $M_1$  beam will have the frequency at which the EIT effect can be produced. Before being guided to MZI, a pump laser is phase locked to  $M_1$  using an off-set

phase lock (OPL), where the offset is the hyperfine splitting between two ground states in  $^{85}\text{Rb}$  atoms, i.e. 3.0357GHz. To keep the MZI fringe at its peak intensity, a square-wave modulation is applied to the AOM, along with  $V_{ref1}$  and the output of the servo after the lock-in amplifier (LIA), denoted as  $V_{FB1}$ . For the other output  $R_2$ , the same procedure is followed, using another SLAUMZI system. Without any rotation, the servo outputs for both  $R_1$  and  $R_2$  are zeroes (mean values). However, in the presence of rotation (around the axis normal to the area of the resonator), the frequencies of the output lasers would deviate from the original values with opposite signs due to the Sagnac effect, which would make  $V_{FB1}$  and  $V_{FB2}$  non-zero. For the case where there is only acceleration (in the direction perpendicular to the diaphragm mounted mirror), the frequency shift in each laser output would be the same. As such, the rate of rotation will be proportional to  $(V_{FB1} - V_{FB2})$ , while the rate of acceleration would be proportional to  $(V_{FB1} + V_{FB2})/2$ .

In the design of such a device, the frequencies of the two Raman lasers can be non-degenerate, differing in frequency by one free spectral range (FSR) of the cavity. This will eliminate the so-called lock-in effect that occurs in a ring laser gyroscope [2], which keeps the two frequencies identical until a sufficiently large rotation occurs. Cumbersome techniques such as mechanical dithering is used to eliminate this effect in a HeNe ring laser gyroscope. Use of the non-degeneracy can eliminate the need for such techniques. The non-degeneracy of the two Raman lasers is illustrated schematically in Figure 3, which corresponds to the left panel in Figure 2.

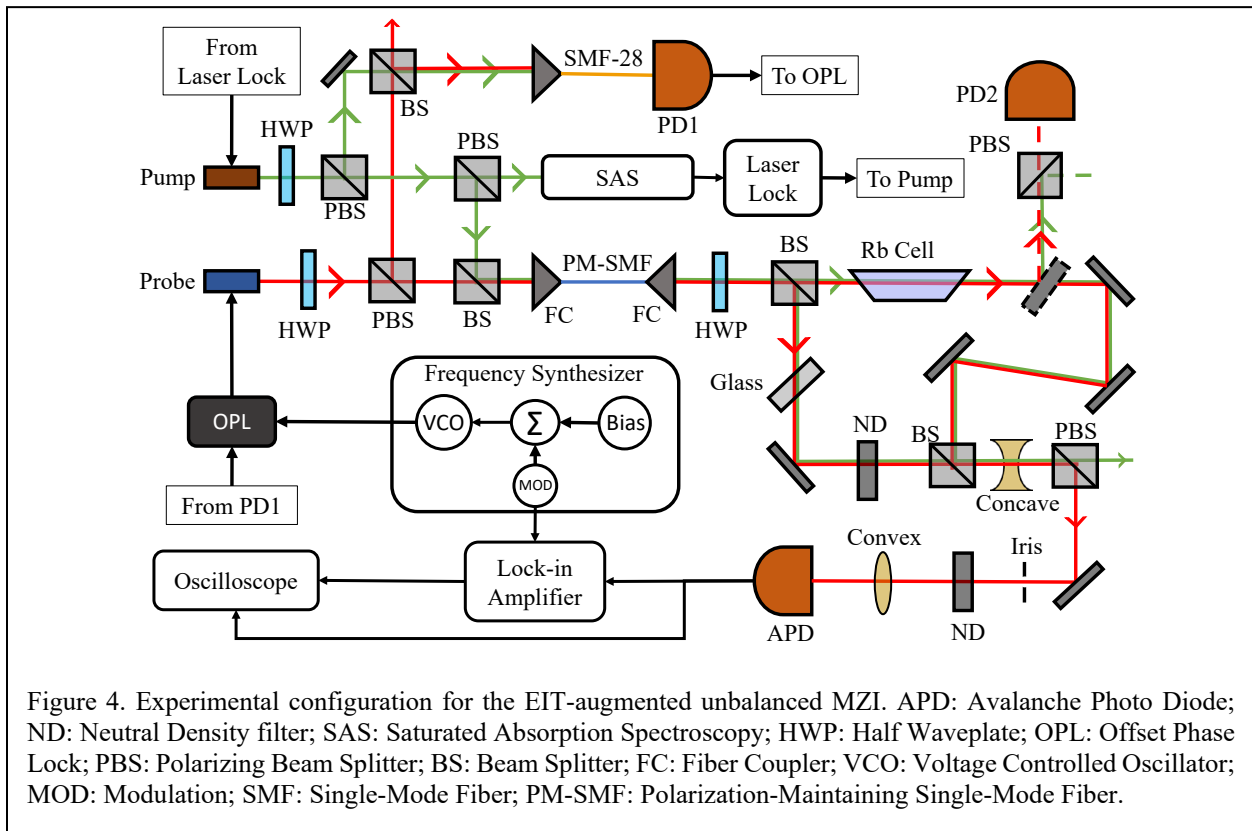


It should be noted that the Raman laser behaves as a subluminal laser [26], which suppresses the sensitivity by the factor of the group index inside the Raman laser. However, according to the theoretical model developed by Henry [20], the STL is reduced by a factor of the square of the group index. For a conventional measurement process, we recall that the MMFS is proportional to the square root of the STL. Thus, the MMFS decreases by a factor of the group index. As such, if Henry's model holds true, then the net frequency sensitivity of Raman laser under conventional detection will be unaffected by the group index inside the Raman laser. An extension of our analysis for the MMFS for the SLAUMZI shows that the group index inside the Raman laser has no effect on our result either, assuming Henry's model holds. Alternatively, the Raman lasers can

be designed to operate superluminally, using any of the various approaches we have demonstrated so far [11,12,13,14,15,16]. In that case, the measurement sensitivity would be further enhanced by the superluminal laser enhancement factor [3,5].

### 3. Experiment

Our primary objective is to demonstrate significant reduction in the MMFS using a SLAUMZI apparatus. However, as we discussed above, it is also possible to reduce the MMFS by using simply an UMZI. As such, we constructed a SLAUMZI in a manner that allows us to vary the group index from a few thousand down to unity, corresponding to an UMZI. This approach has made it possible for us to investigate the reduction in the MMFS for both an UMZI and a



SLAUMZI.

Figure 4 shows the layout of the SLAUMZI, in which Electromagnetic Induced Transparency (EIT) is utilized for generating the slow-light effect. EIT is a two-photon process that can produce a group index as large as  $\sim 1.8 \times 10^7$  [31]. It employs the use of two co-propagating laser beams passing through a Rb vapor cell, for example, with crossed polarizations. Each laser sees a greatly reduced absorption when the frequency difference between them matches the hyperfine splitting in the ground state. This induced transparency is due to the formation of a dark state. The test laser is denoted as the “probe,” which is off-set phase locked (OPL’d) to another laser, denoted as the “pump.” The OPL system takes two inputs, which are the beat signal from the fiber-coupled

photodetector (PD1) and the signal from the frequency synthesizer. The feedback from the OPL system is applied to the probe laser current controller. As such, the frequency synthesizer controls the frequency difference between the two lasers, which nominally matches the frequency difference ( $\sim 3.0357$  GHz) between the hyperfine states  $5S_{1/2} F=2$  and  $5S_{1/2} F=3$  in  $^{85}\text{Rb}$ , and can be tuned around this value. The frequency of the pump laser is locked to the optical transition  $5S_{1/2} F=2$  to  $5P_{1/2} F'=3$  via saturated absorption spectroscopy. A polarization-maintaining single mode fiber (PM-SMF) is used for mode matching of the two lasers. The EIT signal can be monitored by directing the beams to a photodetector (PD2) using a foldable mirror (dashed in the figure), which is removed from the path when the SLAUMZI is operating. On the lower arm of the SLAUMZI, a glass plate is inserted and its position can be adjusted by a PZT-driven holder, in order to adjust the bias phase difference between the paths. To measure the EIT signal, the frequency of the probe laser is swept around the center frequency. In order to minimize the effect of loss of coherence from collisions with the cell walls, we use a paraffin coated vapor cell. The windows are oriented at the Brewster's angle for the probe laser.

A polarizing beam splitter (PBS) is placed after one of the output ports of the SLAUMZI in order to filter out the pump beam. A concave lens followed by an iris is used to monitor signal only from the central fringe. A neutral density filter (ND) is used to reduce the light level to a level below the saturation signal for the avalanche photo diode (APD). The output of the APD is monitored with an oscilloscope, and is also fed to a lock-in amplifier (LIA). The output of the LIA is also monitored directly.

#### a) The Unity Group Index Case

The case where the effect of slow light is not used, corresponding to the group index being unity, is obtained by turning off the EIT in the SLAUMZI, which is achieved by blocking the pump laser and tuning the probe laser away from any absorption. Under this condition, the system operates simply as an UMZI. The probe laser has a linewidth of 376 kHz at  $P_{out} = 0.5$  mW, corresponding to  $\Gamma_L \simeq 2.4 \times 10^6 \text{ sec}^{-1}$ , so that  $\tau_L \simeq 423$  nsec. The values of  $\tau_0$  and  $\tau_D$  were determined to be 1.56 nsec and 0.27 nsec, respectively. Therefore, from Eqn. (33), the SEF in the MMFS is expected to be:

$$R \equiv \frac{\delta\omega_{STD}}{\delta\omega_{UMZI}} = \frac{\tau_{VAC}}{\sqrt{2}} \sqrt{\frac{\sigma N}{\tau_L}} = \frac{\tau_{VAC}}{\sqrt{2}} \sqrt{\frac{\sigma P_0}{\tau_L \hbar \omega}} \approx 161 \quad (34)$$

where  $P_0 = 1.6$  mW is the power of the probe laser before entering the UMZI, and  $\sigma = 1$ . This result implies that the UMZI without slow light is expected to be able to measure a frequency shift that is a factor of  $\sim 161$  times smaller than what can be achieved using the standard technique.

For the APD used in the UMZI output, the quantum efficiency is  $\sim 0.5$ . However, various auxiliary optical elements were used between the output of the UMZI and the input plane of the detector, including several lenses, a polarizing beam splitter, an aperture and a neutral density filter, in order not to exceed the low saturation intensity of the APD. When effects of these elements are taken into account, we determine the value of  $\eta_{eff}$  to be  $\sim 1.63 \times 10^{-4}$ . Thus, for fair

comparison, we will assume this value of the quantum efficiency for both the standard technique and the UMZI technique. Of course, it should be possible to eliminate the use of these auxiliary elements in a potentially practical version of the SLAUMZI sensor for measuring frequency shift, in a manner so that the quantum efficiency would be determined primarily by that of the detector.

The measurement bandwidth,  $\Gamma_M$ , is given by the bandwidth of the Lock-in Amplifier, which is  $\sim 20.7 \text{ sec}^{-1}$ , since it is slower than the APD, which has a bandwidth of  $\sim 50 \text{ MHz}$ . Given the value of  $\Gamma_L$  mentioned above, the MMFS for the standard technique according to Eq.(32) would be:

$$\delta\omega_{STD} = \sqrt{\frac{\Gamma_L \Gamma_M}{\eta_{eff}}} = \sqrt{\frac{2.4 * 10^6 * 20.7}{1.63 * 10^{-4}}} \approx 5.5 * 10^5 \text{ sec}^{-1} \quad (35)$$

Since the SEF estimated above is  $\sim 161$ , we would then expect that the MMFS for the UMZI would be:

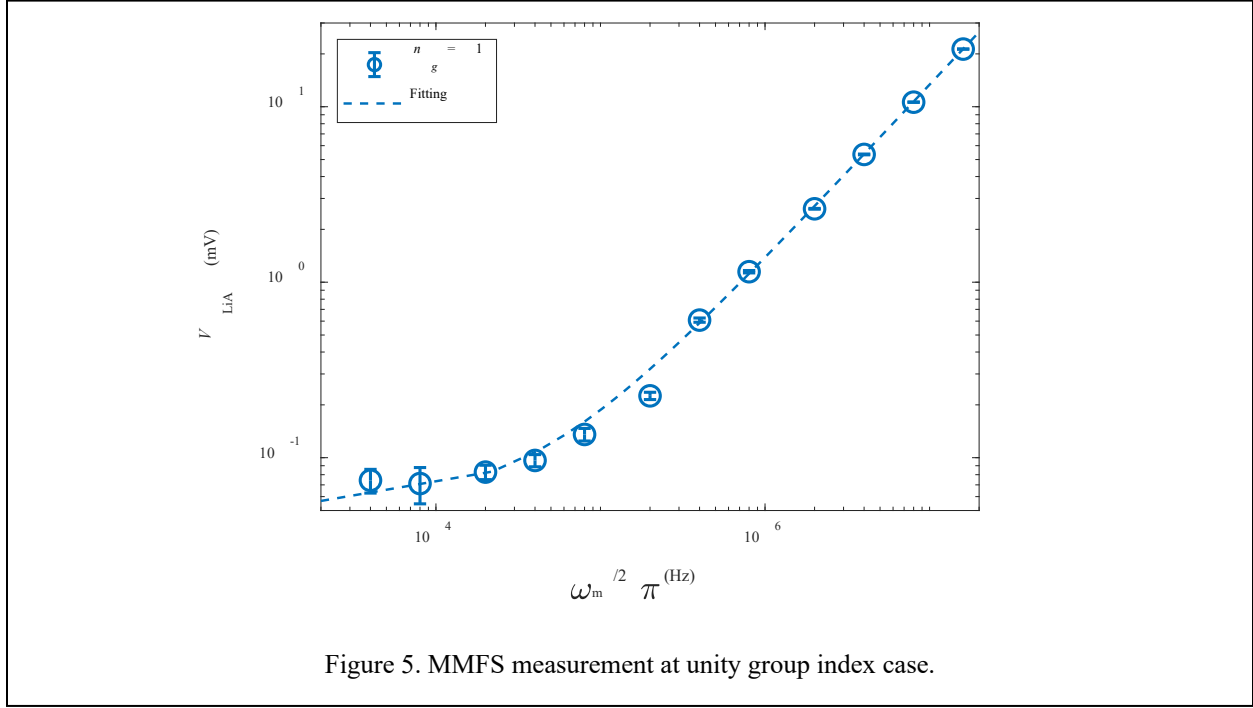
$$\delta\omega_{UMZI} = \frac{\delta\omega_{STD}}{R} \approx 3.4 * 10^3 \text{ sec}^{-1} \quad (36)$$

We measured the MMFS for the UMZI by modulating the probe frequency and monitoring the demodulated signal. Specifically, the probe frequency was modulated around its quiescent value using a square wave. The glass plate was adjusted to maximize the signal modulation observed by the APD at the output port, thus ensuring operation at the point where the slope of the fringe is maximum. The APD signal was then fed into the LIA and demodulated after optimizing its phase. The swing in the laser frequency, denoted as  $\omega_m$ , due to the application of the square wave



modulation, was varied while observing the LIA output. The scaling of  $\omega_m$  was calibrated separately by monitoring the output of the frequency synthesizer using a spectrum analyzer.

Figure 5 shows the output of the LIA, denoted as  $V_{LIA}$ , as a function of the frequency swing,  $\omega_m$ . To model the system, we assume an ideal LIA output without any noise, so that:



$$V_{ideal} = k \frac{\omega_m}{2\pi} \quad (37)$$

where  $V_{ideal}$  is the ideal LIA output without any noise, and  $k$  is the coefficient which can be obtained by fitting the linear part of the experimental data. The effect of excess noise is modeled as a constant parameter in the LIA, the magnitude of which can be adjusted to give the best fitting result. If we denote the noise as  $V_N$ , the total output can be written as:

$$V_{fit} = k \frac{\omega_m}{2\pi} + V_N \quad (38)$$

Therefore, corresponding to each frequency deviation  $\omega_m$  in the experiment, the difference between the fitting value and the experimental value can be defined as:

$$\Delta V_{diff} \equiv V_{LIA} - V_{fit} = V_{LIA} - \left( k \frac{\omega_m}{2\pi} + V_N \right) \quad (39)$$

Here we further define the sum of the square of the ratio between the difference and the LIA output as  $K_{sum}$ , which is written as:

$$K_{sum} = \sum_m \left[ \Delta V_{diff} \left( \frac{\omega_m}{2\pi} \right) / V_{LIA} \left( \frac{\omega_m}{2\pi} \right) \right]^2 = \sum_m \left\{ \left[ V_{LIA} \left( \frac{\omega_m}{2\pi} \right) - k \frac{\omega_m}{2\pi} - V_N \right] / V_{LIA} \left( \frac{\omega_m}{2\pi} \right) \right\}^2 \quad (40)$$

By minimizing the value of  $K_{sum}$ , we determine the value of  $V_N$  to be  $\sim 0.054$  mV. Figure 5 shows the best fitting curve found by implementing the process described above. The linear part of this fit yields the value of  $k$  to be  $\sim 2.2 \cdot 10^{-7}$  mV/sec. The MMFS is then defined as the frequency at which the ideal signal equals the noise level:  $V_{ideal} = V_N$ . Applying this criterion, we get the MMFS for the SLAUMZI system to be

$$\delta\omega_{UMZI} = V_N / k \approx 2.45 \cdot 10^5 \text{ sec}^{-1} \quad (41).$$

As can be seen comparing this value with the one shown in Eqn. (36), the experimentally measured value of the MMFS is larger by a factor of  $\sim 72$ . This discrepancy is due to the fact that the excess noise in the system is dominant over shot noise, as discussed in **Supplement II**.

In order to minimize the effect of the excess noise, we made several changes to the experimental conditions. First, the UMZI was fine tuned for a better alignment, which eliminates the need for the concave lens and the iris after the combining port of the UMZI. Second, the need for using the neutral density (ND) filter in front of the APD was also eliminated, by limiting the light power coming into the UMZI to be small enough not to exceed the detection threshold of the APD. As a result, the effective quantum efficiency in Eq. (35) is now the same as the quantum efficiency of the detector only. Third, we changed the scheme for modulating the laser frequency. Instead of using the OPL system, which produced additional noise, we modulated the laser current directly, by a 10-kHz sinusoidal function, the amplitude of which determines the frequency shift in the laser. Figure 6(a) shows the modified scheme.

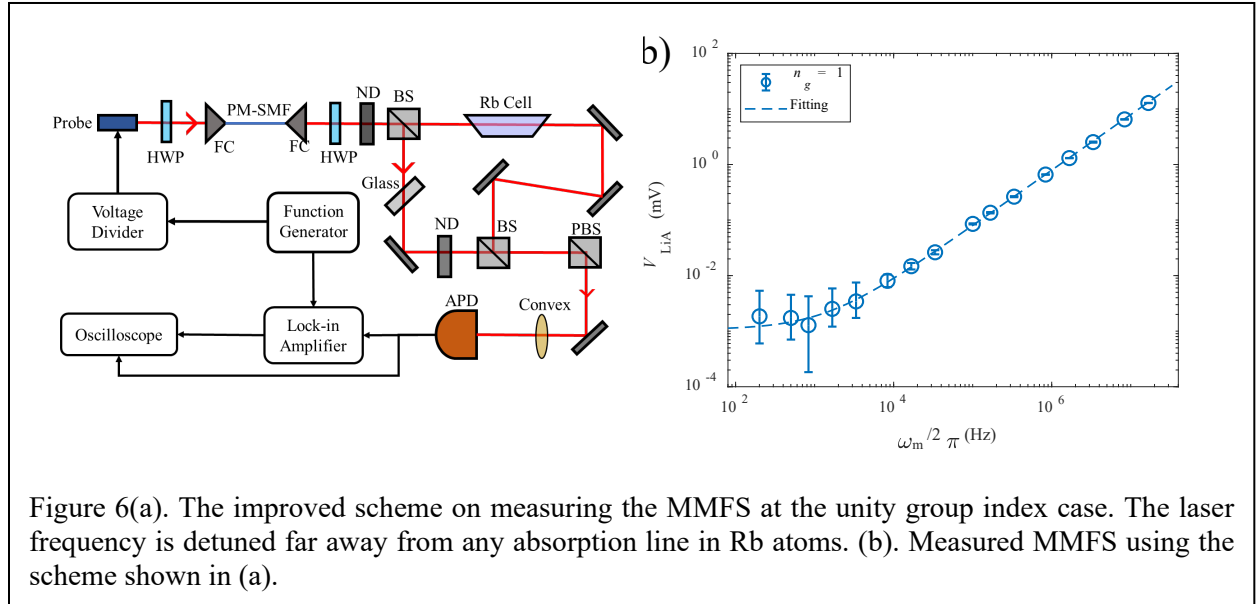


Figure 6(b) shows the data from the MMFS measurement. The parameters used for the data shown here are the same as used earlier, except that the input power is much lower:  $P_0 = 0.73 \mu\text{W}$ . The MMFS for the standard technique is then:

$$\delta\omega_{STD} = \sqrt{\frac{\Gamma_L \Gamma_M}{\eta_d}} = \sqrt{\frac{2.4 * 10^6 * 20.7}{0.5}} \approx 9.97 * 10^3 \text{ sec}^{-1} \quad (42)$$

From Eqn. (34), it follows that the enhancement in the MMFS is  $\sim 3.4$ . As such, the expected MMFS for the UMZI is  $\sim 2.93 * 10^3 \text{ sec}^{-1}$ . Following the same analysis procedure as stated before, the value of  $V_N$  is determined to be  $\sim 0.0011 \text{ mV}$  and the value of  $k$  to be  $\sim 1.26 * 10^{-7} \text{ mV/sec}$ . Therefore, the MMFS corresponding to the unity signal-to-noise ratio is found to be  $\sim 8.73 * 10^3 \text{ sec}^{-1}$ . This is larger than the expected value by a factor of  $\sim 3$ , which is a significant improvement compared to the initial experiment summarized in Figure 5, for which the experimentally observed value of the MMFS was larger than the expected value by a factor of  $\sim 71$ .

It should be noted that the difference between the expected MMFS's for the UMZI, before and after the modification, is due solely to the fact that the input powers ( $P_0$ ) are different for these cases. Recalling briefly, the power that is received by the APD needs to be lower than its saturation power. In the case shown in Figure 5, the input power is set high (1.5 mW) before the UMZI and is attenuated by the ND filter before the detection, which makes the effective quantum efficiency much smaller than the quantum efficiency of the detector. On the other hand, for the case shown in Figure 6, because of the elimination of the ND filter, the input power needs to be set low enough before the UMZI so that the APD is not saturated. Thus, even though the modified scheme has a much higher quantum efficiency, the MMFS remains small.

In order to circumvent this constraint, we need to employ a detection scheme for which there would be no need to reduce the input power. As shown in Section 2 in **Supplement II**, a carefully designed balanced detector can have a higher saturation power than an APD does, which allows a higher input power to the UMZI, while also being capable of suppressing the intensity noise that is significantly larger than the shot noise at such input power. Assuming a detection quantum efficiency of 0.5, this approach would yield an MMFS of  $62 \text{ sec}^{-1}$  in case of Figure 5. We will implement this approach in the near future.

## **b) The EIT case**

The EIT case is established by unblocking the pump laser, tuning the probe laser to become two-photon resonant with the hyperfine ground states, and off-set phase locking the probe to the pump. The power ratio between the pump and the probe lasers and the number density of Rb atoms are varied in order to generate different values of the group index, which can be inferred from the corresponding fringe magnification factor  $M$ . To characterize the fringe magnification due to the EIT process, we applied a square wave modulation at 200 kHz to the OPL, which causes the frequency of the probe beam to be modulated. This signal is also used as the external reference for the LIA. We adjust the glass plate until the amplitude of the modulation observed at the APD output is maximized, corresponding to operating at a point on the fringe with the maximum slope.

Then the modulation signal is compared with the amplitude of the modulation signal in the absence of the EIT effect, which corresponds to the group index being unity.

The fringe magnification factor can be expressed as:

$$M = \left| \frac{(\Delta V_{pp}^{\max})_{EIT}}{(\Delta V_{pp}^{\max})_{UGI}} \right| \quad (43)$$

where  $(\Delta V_{pp}^{\max})_{EIT}$  and  $(\Delta V_{pp}^{\max})_{UGI}$  are the maximized peak-to-peak values of the signal in the EIT and unity group index cases, respectively. We have implemented five different cases of EIT for the SLAUMZI apparatus. In what follows, we present first the results from four of the five cases. The last one, which yielded that largest group index, is presented later.

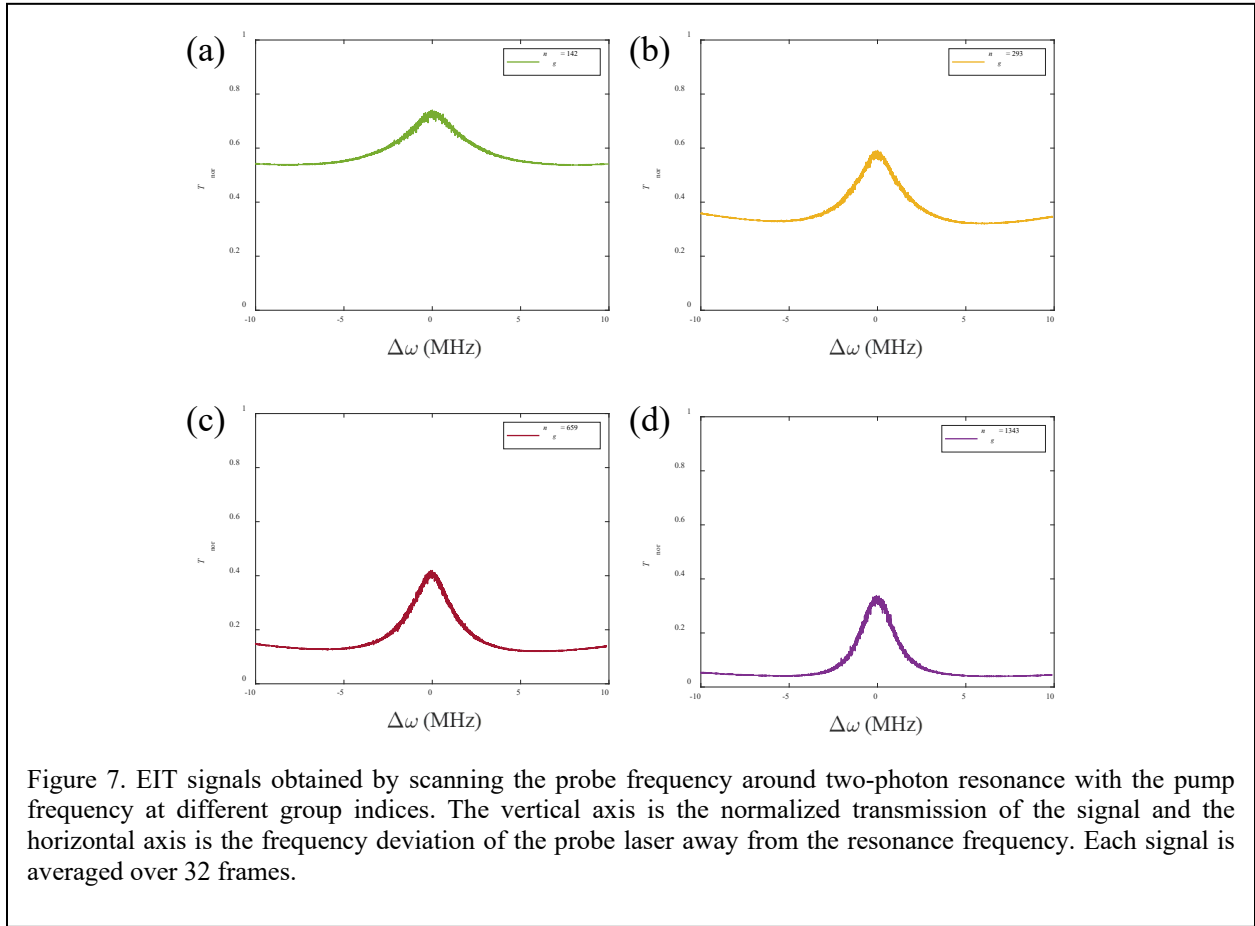


Figure 7 shows four different EIT signals. The magnification factors for these cases are found to be 22, 43, 97 and 196. The inferred values of the corresponding group indices are 142, 293, 659 and 1343, respectively, based on Eq. (3). The input probe power is  $P_0 = 1.2$  mW for  $n_g = 142, 293, 659$  and  $P_0 = 1.6$  mW for  $n_g = 1343$ . Therefore, the SEFs are expected to be:

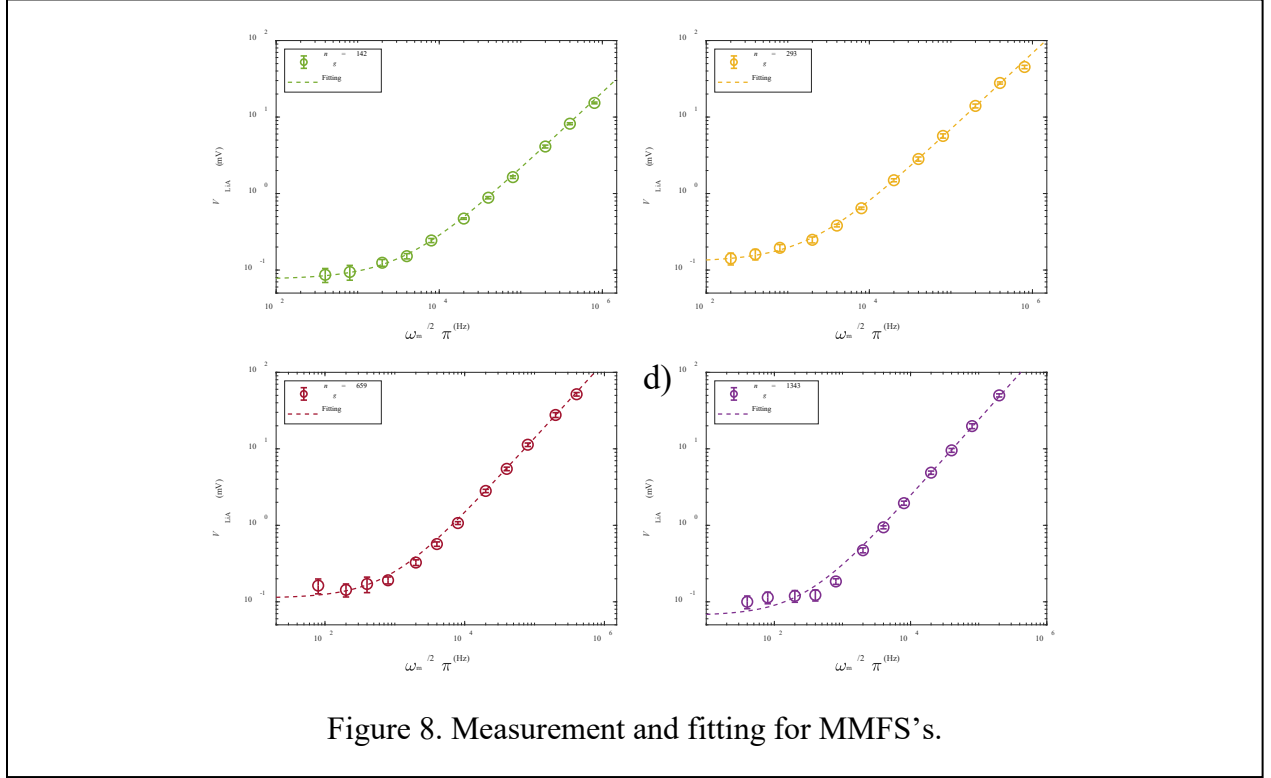
$$\begin{aligned}
R(n_g = 142) &= \frac{\tau_{SL1}^{EIT}}{\sqrt{2}} \sqrt{\frac{\sigma_1 P_0}{\tau_L \hbar \omega}} \approx 2.6 * 10^3 \\
R(n_g = 293) &= \frac{\tau_{SL2}^{EIT}}{\sqrt{2}} \sqrt{\frac{\sigma_2 P_0}{\tau_L \hbar \omega}} \approx 4.7 * 10^3 \\
R(n_g = 659) &= \frac{\tau_{SL3}^{EIT}}{\sqrt{2}} \sqrt{\frac{\sigma_3 P_0}{\tau_L \hbar \omega}} \approx 8.7 * 10^3 \\
R(n_g = 1343) &= \frac{\tau_{SL4}^{EIT}}{\sqrt{2}} \sqrt{\frac{\sigma_4 P_0}{\tau_L \hbar \omega}} \approx 1.8 * 10^4
\end{aligned} \tag{44}$$

where  $\tau_{SL1}^{EIT} = 39.4nsec$ ,  $\tau_{SL2}^{EIT} = 79.7nsec$ ,  $\tau_{SL3}^{EIT} = 177.2nsec$  and  $\tau_{SL4}^{EIT} = 360.0nsec$  are the slow light time delays and  $\sigma_1 = 0.78$ ,  $\sigma_2 = 0.6$ ,  $\sigma_3 = 0.42$  and  $\sigma_4 = 0.33$  are the normalized transmission at the center frequency for each group index, respectively.

As we discussed earlier (see Eqn. (34) to Eqn. (36)) in the case of the unity group index, the actual value of the MMFS is strongly affected by the fact that the effective quantum efficiency of the detection process is very small due to experimental constraints. For a fair comparison, we assume that the effective quantum efficiency for the standard technique to be the same. For the four EIT cases, the effective quantum efficiencies are  $2*10^{-4}$ ,  $4*10^{-4}$ ,  $5.5*10^{-4}$  and  $5*10^{-4}$ . Using these values, we can infer that the theoretical values of the MMFS's for the four EIT cases would be:

$$\begin{aligned}
MMFS(n_g = 142) &= 2.0 * 10^2 \text{ sec}^{-1} \\
MMFS(n_g = 293) &= 77 \text{ sec}^{-1} \\
MMFS(n_g = 659) &= 35 \text{ sec}^{-1} \\
MMFS(n_g = 1343) &= 18 \text{ sec}^{-1}
\end{aligned} \tag{45}$$

Experimentally, the MMFS's are measured by following the procedure described in the unity group index case, and the results are shown in Figure 8. The MMFS's are found to be  $2.6 \cdot 10^4 \text{sec}^{-1}$ ,  $1.5 \cdot 10^4 \text{sec}^{-1}$ ,  $4.8 \cdot 10^3 \text{sec}^{-1}$ ,  $1.7 \cdot 10^3 \text{sec}^{-1}$ , respectively, corresponding to group indices



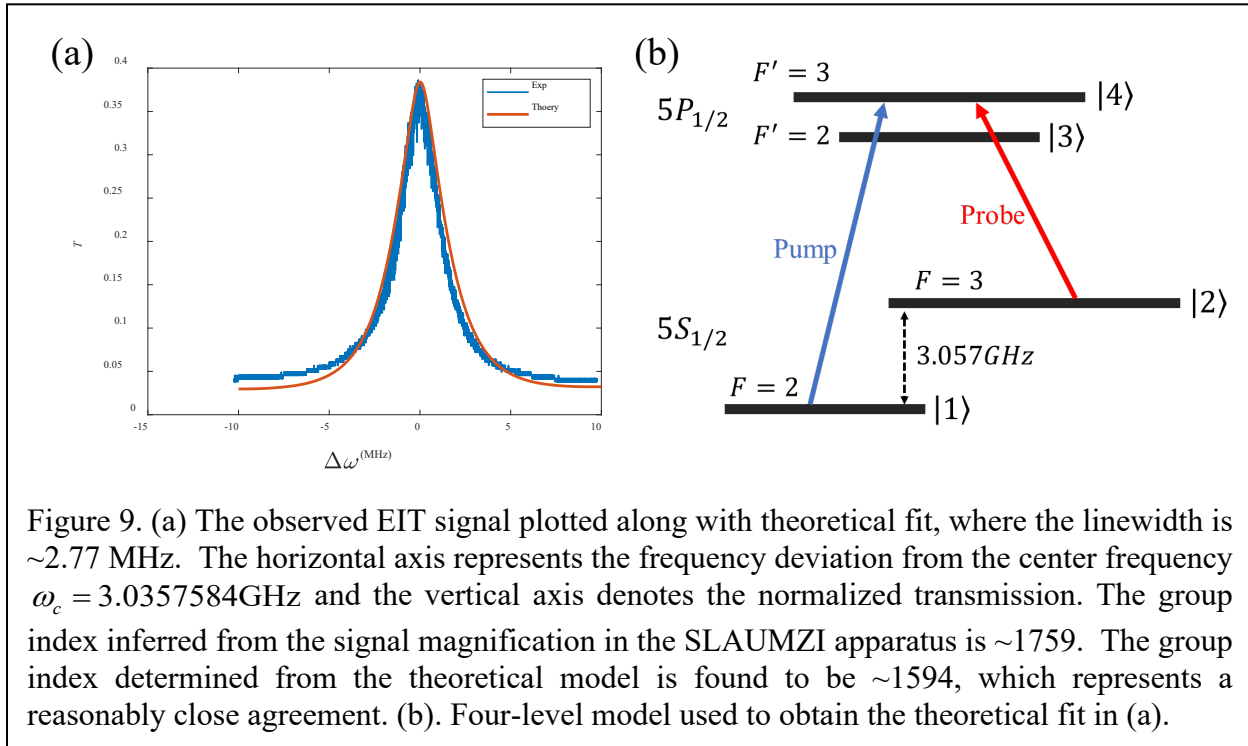
142, 293, 659 and 1343, respectively.

The calculated values of  $V_N$ , which represent the excess noise corresponding to each group index, along with the corresponding values of  $k$ , are displayed in Table 1. Thus, the MMFS's that take into account the excess noise can be also be determined, as shown in the same table. The observed SEF for each case, shown in the last row in Table 1. is given by the ratio of the MMFS for the standard technique and the experimentally measured MMFS in SLAUMZI.

$n_g$	142	293	659	1343
$V_N$ (mV)	0.080	0.14	0.10	0.066
$k$ (mV/sec)	$3.1 \cdot 10^{-6}$	$9.5 \cdot 10^{-5}$	$2.1 \cdot 10^{-5}$	$3.8 \cdot 10^{-5}$
MMFS (EIT, Experiment)	$2.6 \cdot 10^4 \text{ sec}^{-1}$	$1.5 \cdot 10^4 \text{ sec}^{-1}$	$4.8 \cdot 10^3 \text{ sec}^{-1}$	$1.7 \cdot 10^3 \text{ sec}^{-1}$
MMFS (EIT, Theory)	$1.2 \cdot 10^3 \text{ sec}^{-1}$	$4.8 \cdot 10^2 \text{ sec}^{-1}$	$2.1 \cdot 10^2 \text{ sec}^{-1}$	$1.1 \cdot 10^2 \text{ sec}^{-1}$
MMFS(STD)	$5.0 \cdot 10^5 \text{ sec}^{-1}$	$3.5 \cdot 10^5 \text{ sec}^{-1}$	$3.0 \cdot 10^5 \text{ sec}^{-1}$	$3.2 \cdot 10^5 \text{ sec}^{-1}$
SEF(Observed)	19	24	63	185

Table 1. The MMFS's obtained from fitting to the experimental data and their corresponding  $V_N$ . The theoretical MMFS's, for both SLAUMZI and standard technique, are also listed for reference. The observed sensitivity enhancement factors (SEF) is the ratio of the MMFS predicted for the standard technique (row 6) and the experimentally observed MMFS (row 4).

Figure 9(a) shows the EIT signal for the case that yielded the largest value of the group index. We have used a 4-level system to model the EIT effect, as illustrated in Figure 9(b), by



solving the Liouville equations using the N-level algorithm developed by our group [33]. The pump laser couples the hyperfine state  $5S_{1/2} F=2$  (state  $|1\rangle$ ) to the  $5P_{1/2}$  manifold, which consists of two hyperfine states  $5P_{1/2} F'=2$  (state  $|3\rangle$ ) and  $5P_{1/2} F'=3$  (state  $|4\rangle$ ). The probe laser couples

the states  $5S_{1/2} F=3$  (state  $|2\rangle$ ) and the  $5P_{1/2}$  manifold. The pump Rabi frequencies for the 1-3 and 1-4 transitions are  $\Omega_{13} = 3.2 \cdot 10^7 \text{ sec}^{-1}$  and  $\Omega_{14} = 3.4 \cdot 10^7 \text{ sec}^{-1}$ , respectively. The probe Rabi frequencies for the 2-3 and 2-4 transitions are  $\Omega_{23} = 3.1 \cdot 10^7 \text{ sec}^{-1}$  and  $\Omega_{24} = 4.3 \cdot 10^7 \text{ sec}^{-1}$ , respectively. The decay rates for the 3-1 and 3-2 transition are determined by their relative ratio of the rabi frequency and are found to be  $1.8 \cdot 10^7 \text{ sec}^{-1}$  and  $1.8 \cdot 10^7 \text{ sec}^{-1}$ , respectively. Similarly, the decay rates for the 4-1 and 4-2 transition are  $2.7 \cdot 10^7 \text{ sec}^{-1}$  and  $0.9 \cdot 10^7 \text{ sec}^{-1}$ , respectively. The collisional decay rates between the two ground states  $|1\rangle$  and  $|2\rangle$  are assumed to be the same for both directions and are  $3.76 \cdot 10^6 \text{ sec}^{-1}$ . The Rb cell temperature used in the model is 70 degree Celsius and the length of the cell is 0.08 m. The Doppler broadening is also accounted for by averaging the signal over different velocity groups. Moreover, since the absorption is significant, we implement the cell slicing technique in our model, in which we slice the Rb cell into 10 segments and calculate the intensity of the incident light after each slice. The group index inferred from the signal magnification in the SLAUMZI apparatus is  $\sim 1759$ . The group index determined from the theoretical model is found to be  $\sim 1594$ , which represents a reasonably close agreement.

The measured fringe magnification factor is  $M \sim 257$ . Using Eq.(3), with  $\tau_0 = 1.56 \text{ nsec}$  and  $\tau_D = 0.27 \text{ nsec}$ , the value of  $\tau_{SL}$  is found to be  $\sim 471 \text{ nsec}$ . Given the input power  $P_0 = 1.6 \text{ mW}$  and absorption coefficient  $\sigma = 0.37$ , the enhancement in the MMFS is expected to be

$$R \equiv \frac{\delta\omega_{STD}}{\delta\omega_{SLAUMZI}^{EIT}} = \frac{\tau_{SL}}{\sqrt{2}} \sqrt{\frac{\sigma N}{\tau_L}} = \frac{\tau_{SL}}{\sqrt{2}} \sqrt{\frac{\sigma P_0}{\tau_L \hbar \omega}} \approx 2.5 \cdot 10^4. \quad (46)$$

This result implies that at this operating condition, the SLAUMZI is expected to be able to measure a frequency shift that is a factor of  $\sim 2.5 \cdot 10^4$  times smaller than what can be achieved using the standard technique. The value of the effective quantum efficiency is determined to be

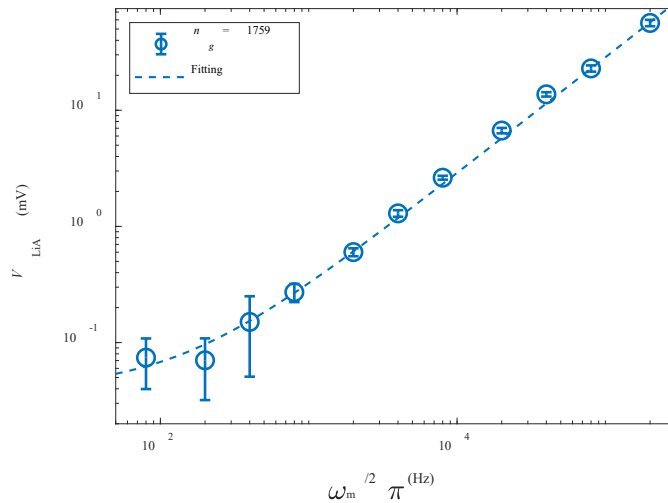


Figure 10. The output of the Lock-in amplifier as a function of the FM frequency deviation.



$\sim 2.95 \times 10^{-4}$ . Given the same  $\Gamma_M$  and  $\Gamma_L$  mentioned above, the MMFS for the standard technique  $\delta\omega_{STD}$  is calculated to be  $\sim 4.1 \times 10^5 \text{ sec}^{-1}$ , so that the MMFS for the SLAUMZI would be  $\sim 16 \text{ sec}^{-1}$ , if we assume a shot-noise limited detection.

Figure 10 shows the results for measuring the MMFS for this case. Using Eq. (38) to fit the data, the MMFS is found to be  $\sim 733 \text{ sec}^{-1}$ , and the measure of the excess noise is found to be  $V_N \sim 0.033 \text{ mV}$ . The value of  $k$  is determined to be  $4.5 \times 10^{-5} \text{ mV/sec}^{-1}$ . Therefore, the observed sensitivity enhancement factor (SEF) is  $\sim 4.1 \times 10^5 / 733 = 560$ .

Similar to the unity group index case, we attempted to carry out the EIT case with a larger value of the effective quantum efficiency, by realigning the UMZI, eliminating the ND filter and the aperture before the APD, and limiting the input power that enters the UMZI to a level ( $< 1.5 \mu\text{W}$ ) that avoids saturating the APD. However, at this power level, the EIT process is highly inefficient, yielding a much lower value of the group index, while increasing the absorption of the probe signal. To circumvent this constraint, it is necessary to replace the APD with a balanced detector, as mentioned at the end of Section 3(a). Furthermore, it should be noted that, as shown in Section 5 in **Supplement II**, the use of the OPL adds additional noise to the system. To eliminate this problem, one can generate the probe beam directly from the pump laser by using an acousto-optic modulator (AOM). We plan to make these modifications to the system in order to demonstrate a much smaller value of the MMFS. More experiments based on the discussion above will be conducted and communicated in the near future.

#### 4. Conclusions

We have demonstrated a slow-light augmented unbalanced Mach-Zehnder interferometer (MZI) which can be used to enhance very significantly the sensitivity of measuring the frequency shift in a laser. We have shown theoretically and verified experimentally that the degree of enhancement depends on the group index of the slow-light medium, the degree of imbalance between the physical lengths of the two arms of the MZI, and the spectral width of the laser. For a laser based on a high-finesse cavity, yielding a narrow quantum noise limited spectral width, the group index has to be larger than the finesse in order to achieve enhancement in measurement sensitivity. For the reported results, strong slow-light effect was produced by employing electro-magnetically induced transparency via coherent population trapping in a buffer-gas loaded vapor cell of Rb atoms, with a maximum group index of  $\sim 1759$ . The observed enhancement in sensitivity for a range of group indices agrees well with the theoretical model. The maximum enhancement factor observed is  $\sim 560$ , and much larger values can be obtained using cold atoms for producing the slow-light effect, for example. We have also shown a specific architecture for enhancing the sensitivity of a gyroscope and accelerometer using bi-directional and non-degenerate Raman lasers employing the slow-light augmented unbalanced MZI. The Raman lasers can be either subluminal or superluminal. In the case when the Raman lasers are superluminal, the sensitivity would be increased further due to the superluminal enhancement effect. More generally, the sensitivity of any sensor that relies on measuring the frequency shift of a laser can be enhanced substantially using this technique. These include, but are not limited to, gyroscopes and accelerometers based

on a conventional ring laser or a superluminal ring laser, and detectors for virialized ultra-light field dark matter.

## Reference

- [1] E. J. Post, "The Sagnac Effect," *Rev. Mod. Phys.* 39, 475 (1967)
- [2] W. W. Chow, J. Gea-Banacloche, L. M. Pedrotti, V. E. Sanders, W. Schleich, and M. O. Scully, "The ring laser gyro," *Reviews of Modern Physics* 57, 61 (1987)
- [3] M. S. Shahriar, G. S. Pati, R. Tripathi, V. Gopal, and M. Messall, "Ultrahigh enhancement in absolute and relative rotation sensing using fast and slow light," *Phys. Rev. A* 75, 053807-1 - 053807-10 (2007).
- [4] A. A. Geraci, C. Bradley, D. Gao, J. Weinstein, and A. Derevianko, "Searching for Ultralight Dark Matter with Optical Cavities," *Phys. Rev. Lett.* 123, 031304 (2019).
- [5] H. N. Yum, M. Salit, J. Yablon, K. Salit, Y. Wang, and M. S. Shahriar, "Superluminal ring laser for hypersensitive sensing," *Opt. Express* 18(17), 17658 (2010).
- [6] J. Scheuer and S.M. Shahriar, "Lasing dynamics of super and sub luminal lasers", *Opt. Express* 23, 32350– 32365 (2015)
- [7] Y. Wang, Z. Zhou, J. Yablon, and M. S. Shahriar, "Effect of Multi-Order Harmonics in a Double-Raman Pumped Gain Medium for a Superluminal Laser," *Opt. Eng.* 54(5), 057106 (2015).
- [8] J. Yablon, Z. Zhou, M. Zhou, Y. Wang, S. Tseng, and S.M. Shahriar, "Theoretical modeling and experimental demonstration of Raman probe induced spectral dip for realizing a superluminal laser," *Optics Express*, Vol. 24, No. 24, 27446 (2016)
- [9] M. Zhou, Z. Zhou, M. Fouda, N.J. Condon, J. Scheuer, and M.S. Shahriar, "Fast-light Enhanced Brillouin Laser Based Active Fiber Optic Sensor for Simultaneous Measurement of Rotation and Strain," *Journal of Lightwave Technology*, 35 (23), 5222 (2017).
- [10] M.F. Fouda, M. Zhou, H.N. Yum, and S.M. Shahriar, "Effect of cascaded Brillouin lasing due to resonant pumps in a superluminal fiber ring laser gyroscope," *Opt. Eng.* 57(10), 107108 (2018)
- [11] Z. Zhou, M. Zhou and S.M. Shahriar, "A superluminal Raman laser with enhanced cavity length sensitivity," *Optics Express* 27, 29739-29745 (2019)
- [12] Y. Sternfeld, Z. Zhou, J. Scheuer, and M. S. Shahriar, "Electromagnetically induced transparency in Raman gain for realizing a superluminal ring laser," *Opt. Express* 29, 1125-1139 (2021).
- [13] Zifan Zhou, Nicholas Condon, Devin Hileman, and M. S. Shahriar, "Observation of a highly superluminal laser employing optically pumped Raman gain and depletion," *Opt. Express* 30, 6746-6754 (2022).
- [14] Z. Zhou, R. Zhu, N. Condon, D. Hileman, J. Bonacum and S.M. Shahriar, "Bi-directional Superluminal Ring Lasers without Cross-talk and Gain Competition," *Appl. Phys. Lett.* 120, 251105 (2022)
- [15] Z. Zhou, R. Zhu, Y. Sternfeld, J. Scheuer, J. Bonacum, and S. M. Shahriar, "Demonstration of a Superluminal Laser using Electromagnetically Induced Transparency in Raman Gain," *Opt. Express* 31(9), 14377-14388 (2023)
- [16] Y. Sternfeld, Z. Zhou, S.M. Shahriar and J. Scheuer, "Single-pumped gain profile for a superluminal ring laser," *Optics Express* 31(22) 36952-36965 (2023)
- [17] Z. Shi, Robert, W. Boyd, Daniel J. Gauthier, and C. C. Dudley, "Enhancing the spectral sensitivity of interferometers using slow-light media," *Opt. Lett.* 32, 915-917 (2007).
- [18] It is also possible to realize the SLAUI process in a Fabry-Perot Cavity (FPC), based on the fact that the effective path length is different for different orders of multiple reflections. However, the details of the SLAUI process in an FPC is significantly different from those in the MZI and the MI. We will present studies of the SLAUI process in an FPC in the near future.
- [19] C.H. Townes, "Some applications of optical and infrared masers," in *Advances in Quantum Electronics*, J.R. Singer, Ed., New York: Columbia Univ. Press, 1961, pp 1-11.
- [20] C. H. Henry, "Theory of the Linewidth of Semiconductor Lasers," *IEEE J. Of Quantum Electronics*, Vol. QE-18, No. 2, (1982)
- [21] T.A. Dorschner, H.A. Haus, M. Holz, I.W. Smith, H. Statz, "Laser gyro at quantum limit", *IEEE J. Quant. Elect.* QE-16, 1376 (1980)
- [22] B. T. King, "Application of superresolution techniques to RLGs: exploring the quantum limit," *Applied Optics* 39, 6151 (2000).

- 
- [23] M. O. Scully and M.S. Zubairy, Quantum Optics, Cambridge University Press (1997).
- [24] J. Capmany, J. Mart and H. Mangraham, "Impact of Finite Laser Linewidth on the Performance of OFDM Networks Employing Single-Cavity Fabry-Perot Demultiplexers," Journal of Lightwave Technology, vol. 13, no. 2 (1995).
- [25] F. Aronowitz, in Laser Applications, edited by M. Ross (Academic, New York) pp. 113-200.
- [26] J. Yablon, Z. Zhou, N. J. Condon, D. J. Hileman, S. C. Tseng, and M.S. Shahriar, "Demonstration of a highly subluminal laser with suppression of cavity length sensitivity by nearly three orders of magnitude." Optics Express, 25 (24), 30327 (2017).
- [27] W. M. Itano, J. C. Bergquist, J. J. Bollinger, J. M. Gilligan, D. J. Heinzen, F. L. Moore, and D. J. Wineland, "Quantum projection noise: Population fluctuations in two-level systems," Phys. Rev. A 47, 3554 (1993).
- [28] In order to account for the effect of the absorption from a phase insensitive process, as well as the sub-unity quantum efficiency of a intensity-measuring detector, one can formulate an equivalent ideal beamsplitter for each case, where the degree of attenuation is accounted for by the finite transmittivity of the beam splitter, and a vacuum mode is added at the free port in order to ensure that the output satisfies the Bosonic commutation relations [29,30]. However, when the input fields being attenuated are much stronger than the vacuum mode, the result would become essentially equivalent to the simple model we have used here [30].
- [29] C.M. Caves, "Quantum limits on noise in linear amplifiers," Phys. Rev. D 26, 8, 1817 (1982).
- [30] B.L. Schumaker, "Noise in Homodyne Detection," Optics Letters, Vol 9, No. 5, 189 (1984)
- [31] L.V. Hau, S. E. Harris, Z. Dutton and C. H. Behrooz, "Light speed reduction to 17 metres per second in an ultracold atomic gas," Nature 397, 18 (1999).
- [32] A. V. Turukhin, V.S. Sudarshanam, M.S. Shahriar, J.A. Musser, B.S. Ham, and P.R. Hemmer, "Observation of Ultraslow and Stored Light Pulses in a Solid," Phys. Rev. Lett. 88, 023602 (2001)
- [33] M. S. Shahriar, Y. Wang, S. Krishnamurthy, Y. Tu, G. S. Pati and S. Tseng, "Evolution of an N-level system via automated vectorization of the Liouville equations and application to optically controlled polarization rotation," Journal of Modern Optics, 61:4, 351-367 (2014)

## Supplement I: Analysis of MMFS

In the main body of the paper, we have argued that the use of the SLAUMZI can greatly reduce the minimum measurable frequency shift (MMFS) when compared to the heterodyne technique, where a reference laser with an infinitely narrow linewidth is mixed with the test laser and the frequency uncertainty is determined by the root mean square (RMS) of the linewidth of the test laser and the measurement bandwidth. In the following, we will show that the MMFS obtained by using the heterodyne technique (also referred as standard case in the following) is not a fundamental limit. For certain parameters, the MMFS that can be achieved by an unbalanced Mach-Zehnder interferometer (UMZI) without employing slow-light can be smaller than the MMFS in the heterodyne technique. At the end of the analysis, we will present a numerical estimate on the condition where the MMFS in UMZI exceeds the MMFS in the standard technique, for experimentally achievable parameters.

### 1. Derivation of the MMFS in the standard case

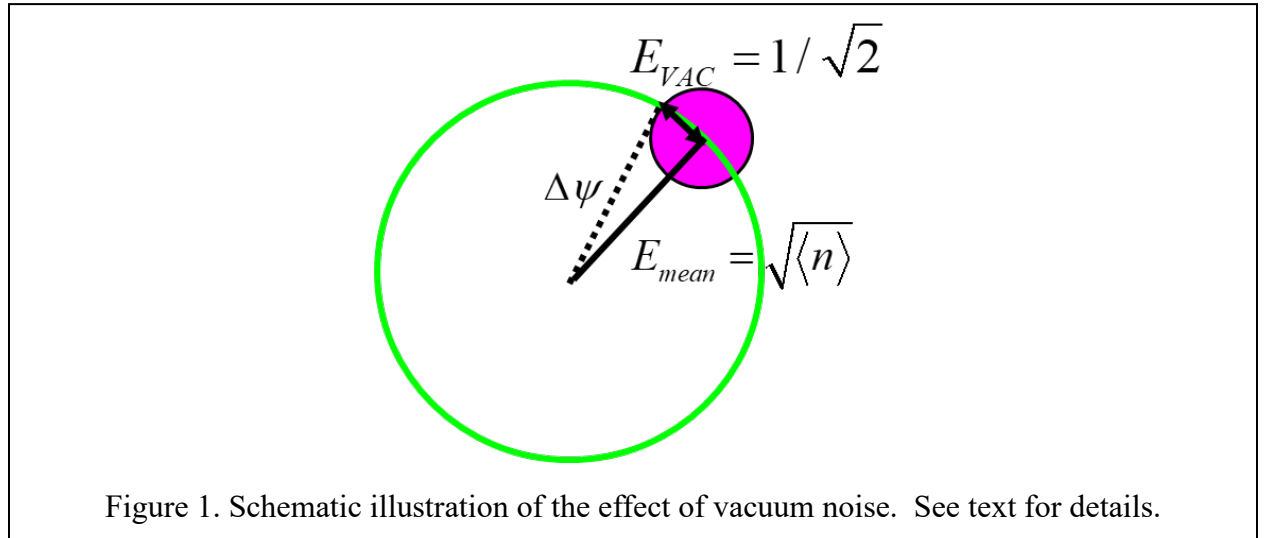
**1.1 Approach 1:** Consider a ring laser with a single output port. The photons inside the cavity decay in a time duration of  $\tau_c$ , the cavity decay time. As such, we can express the mean number of photons inside the laser mode as:

$$\langle n \rangle = [P_{\text{out}} \tau_c / \hbar \omega] \quad (1)$$

We define the mean (dimensionless) electric field amplitude for the laser mode as:

$$\langle \varepsilon \rangle_{\text{laser}} = \sqrt{\langle n \rangle} \quad (2)$$

We assume that the laser mode is in a coherent state, which is a displaced vacuum mode. Therefore,



the mean electric field is accompanied by a randomly phased vacuum mode, as illustrated in Figure 1. The mean electric field (dimensionless) amplitude for this vacuum mode can be written as:

$$\langle \varepsilon \rangle_{\text{vac}} = 1 / \sqrt{2} \quad (3)$$

The phase uncertainty introduced by the vacuum field can be expressed as:

$$\Delta\phi = \frac{\langle \varepsilon_{\text{vac}} \rangle}{\langle \varepsilon_{\text{in}} \rangle} = \frac{1}{\sqrt{2\langle n \rangle}} \quad (4)$$

It should be noted that if the detection system (which is unspecified in this derivation) has a quantum efficiency,  $\eta$ , that is less than unity, then the mean number of photons is effectively reduced by this factor, while the phase fluctuation due to the vacuum mode remains unchanged. As a result, the effective phase uncertainty would be:

$$\Delta\phi = \frac{\langle \varepsilon_{\text{vac}} \rangle}{\langle \varepsilon_{\text{in}} \rangle_{\text{eff}}} = \frac{1}{\sqrt{2\eta\langle n \rangle}} \quad (5)$$

Since the field only lives for a duration of  $\tau_C$ , the resulting spectral noise is given by:

$$\Delta\omega_{\text{min}} = \frac{\Delta\phi}{\tau_C} = \frac{1}{\tau_C} \cdot \sqrt{\frac{\hbar\omega}{2\eta P_{\text{out}} \tau_C}} \quad (6)$$

However, if the measurement is repeated, in a continuous manner,  $N$  times, this averaging process reduces the uncertainty by a factor of  $\sqrt{N}$ . Therefore, we can write:

$$\Delta\omega_{\text{min}}(N\tau_C) = \frac{\sqrt{N\Delta\omega^2(\tau_C)}}{N} = \frac{\Delta\omega(\tau_C)}{\sqrt{N}} = \frac{1}{\tau_C} \cdot \sqrt{\frac{\hbar\omega}{\eta 2P_{\text{out}} \tau_C N}} \quad (7)$$

Since  $N\tau_C = \tau_M$ , the overall spectral noise in a measurement time of  $\tau_M$  is given by:

$$\Delta\omega_{\text{min}}(\tau_M) = \frac{1}{\tau_C} \cdot \sqrt{\frac{\hbar\omega}{\eta 2P_{\text{out}} \tau_M}} \quad (8)$$

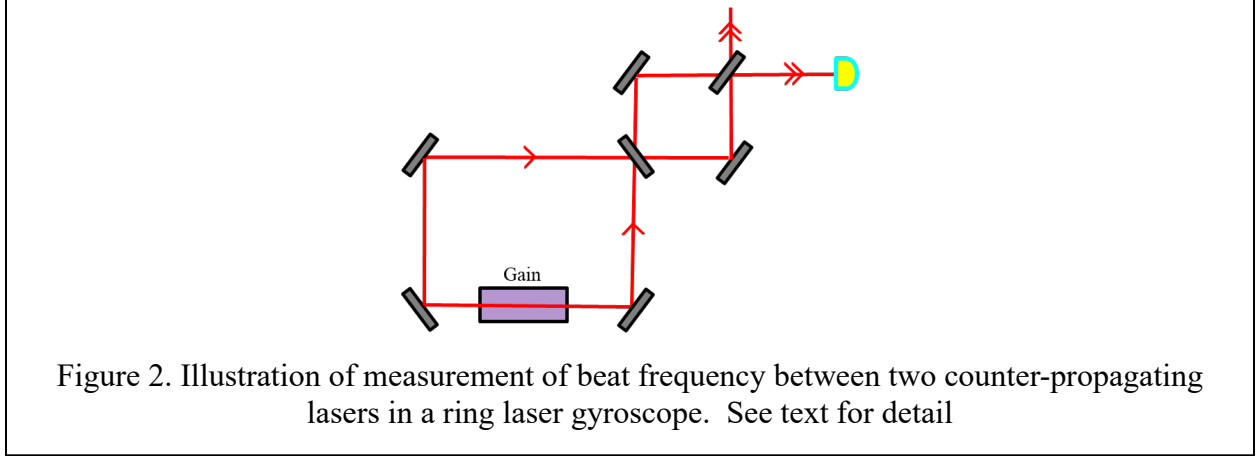
For  $\eta = 1$ , this is in agreement with the expression for the minimum spectral uncertainty in a ring laser gyroscope in references [1] and [2]. The measured spectral uncertainty, for  $\eta = 1$ , is just the geometric mean of the Schwalow-Townes Linewidth (STL) and the measurement bandwidth,  $\gamma_M = \tau_M^{-1}$ :

$$\Delta\omega_{\text{min}}(\tau_M) = \frac{1}{\tau_C} \cdot \sqrt{\frac{\hbar\omega}{2P_{\text{out}} \tau_M}} = \sqrt{\gamma_{\text{STL}} \gamma_M} \quad (9)$$

When the effect of the non-unity quantum efficiency is taken into account, we get:

$$\Delta\omega_{\text{min}}(\tau_M) = \frac{1}{\tau_C} \cdot \sqrt{\frac{\hbar\omega}{\eta 2P_{\text{out}} \tau_M}} = \sqrt{\gamma_{\text{STL}} \gamma_M / \eta} \quad (10)$$

**1.2 Approach 2:** In the derivation shown above, the actual technique for measuring the MMFS is not specified. In what follows, we consider a specific scheme [3] for measuring the MMFS, in the context of a ring laser gyroscope which contains two counter-propagating lasers, illustrated schematically in Figure 2. The analysis in this approach makes use of Langevin noise operators to represent the spectral uncertainty of each laser, and the MMSF is determined by monitoring the



non-zero beat frequency between the two lasers in the presence of rotation which makes the frequencies non-degenerate.

Consider first the property of each laser separately. The time variation of its phase can be expressed as:

$$\psi = \omega_o + \hat{f}(t); \quad \langle \hat{f}(t) \rangle = 0; \quad \langle \hat{f}(t) \hat{f}(t') \rangle = 2D\delta(t-t') \quad (11)$$

where  $\omega_o$  is the mean frequency of the laser,  $\hat{f}(t)$  is a memory-less, delta-correlated Langevin noise operator that represents the phase fluctuation due to white noise, and  $2D$  is the rate of phase diffusion, which equals the spectral width,  $\gamma_L$ , of the laser:

$$2D = \gamma_L \equiv \frac{1}{\tau_L} \quad (12)$$

This is generally true even if the laser linewidth is not fully quantum noise limited (i.e., not the STL), as long as the fluctuations that determine the linewidth are due to white noise. Under quantum noise limit, we have:

$$2D = \gamma_{\text{STL}} = \frac{\hbar\omega_o\gamma_C^2}{2P_{\text{out}}} \equiv \frac{1}{\tau_{\text{STL}}} \quad (13)$$

Consider next the beating of two lasers. The time variation of the phase difference,  $\psi$ , can be written as:

$$\dot{\psi} = \mu + \hat{f}(t) \quad (14)$$

Here,  $\mu$  is the beat frequency, and the Langevin operator obeys the following relations:

$$\langle \hat{f}(t) \rangle = 0; \quad \langle \hat{f}(t) \hat{f}(t') \rangle = 2D' \delta(t - t') \quad (15)$$

Here,  $2D'$  is the sum of the uncorrelated parts of the phase diffusion rates of the two lasers. Under quantum noise limit, and assuming identical properties for both lasers, we can write:

$$2D' = 4D = 2\gamma_{STL} = \frac{\hbar \omega_0 \gamma_C^2}{P_{OUTEL}} \quad (16)$$

where  $P_{OUTEL}$  is the matched output power of each laser. We can integrate Eqn. (14) to write:

$$\psi(t) - \psi(0) = \mu t + \int_0^t \hat{f}(t') dt' \quad (17)$$

Here, the initial phase difference is constant, and can be set to zero for simplicity, so that we can write:

$$\psi(t) = \mu t + \int_0^t \hat{f}(t') dt' \quad (18)$$

It then follows that:

$$\langle \psi(t) \rangle = \mu t + \int_0^t \langle \hat{f}(t') \rangle dt' = \mu t \quad (19)$$

The mean value of the beat frequency is  $\langle \dot{\psi}(t) \rangle = \mu$ . We can calculate the fluctuation in the phase difference as follows:

$$\begin{aligned} \Delta \psi &= \left[ \langle (\psi - \langle \psi \rangle)^2 \rangle \right]^{1/2} = \left[ \left\langle \left\{ \int_0^t \hat{f}(t') dt' \right\}^2 \right\rangle \right]^{1/2} \\ &= \left[ \left\langle \left\{ \int_0^t \hat{f}(t') dt' \right\} \left\{ \int_0^t \hat{f}(t'') dt'' \right\} \right\rangle \right]^{1/2} \\ &= \left[ \int_0^t dt' \int_0^t dt'' \langle \hat{f}(t'') \hat{f}(t') \rangle \right]^{1/2} = \left[ 2D' \int_0^t dt' \int_0^t dt'' \delta(t' - t'') \right]^{1/2} \end{aligned} \quad (20)$$

Noting that since  $0 \leq t' \leq t$ , we have  $\int_0^t dt'' \delta(t' - t'') = 1$ . It then follows that:

$$\Delta \psi = \left[ 2D' \int_0^t dt' \right]^{1/2} = \sqrt{2D't} \quad (21)$$

Thus, the uncertainty in the beat frequency is:

$$\delta\mu = \Delta\psi / t = \sqrt{2D' / t} \quad (22)$$

Denoting the measurement time as  $\tau_M$ , we get the minimum measurable beat frequency as:

$$\delta\mu = \sqrt{\frac{2D'}{\tau_M}} = \sqrt{\frac{2\gamma_{STL}}{\tau_M}} \quad (23)$$

More explicitly, we get (defining  $N_M$  as the total number of photons measured for each laser):

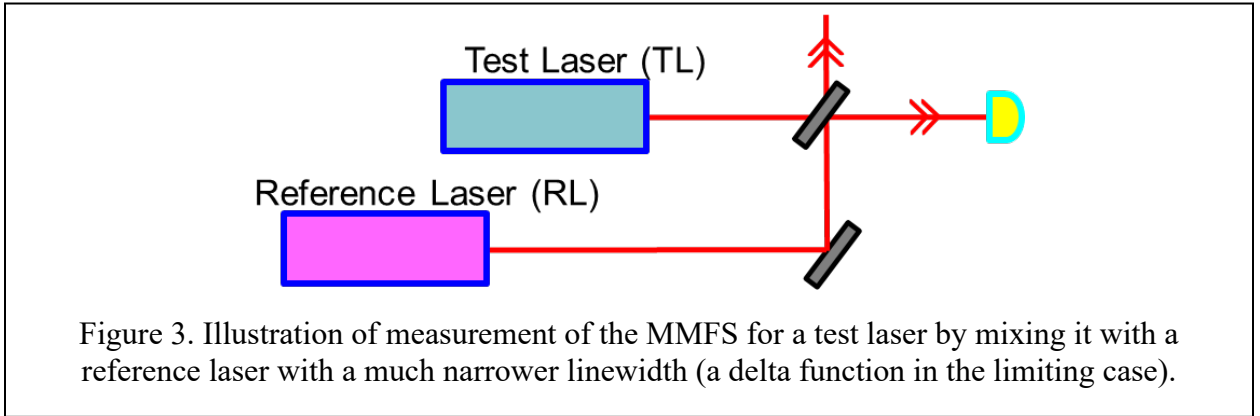
$$\delta\mu = \sqrt{\frac{\hbar\omega_0\gamma_C^2}{P_{OUTEL}\tau_M}} = \frac{\gamma_C}{\sqrt{N_M}} = \frac{1}{\tau_C\sqrt{N_M}} \quad (24)$$

Taking into account the quantum efficiency,  $\eta$ , of the detector, we get:

$$\delta\mu = \frac{1}{\tau_C\sqrt{\eta N_M}} = \sqrt{\frac{\hbar\omega_0\gamma_C^2}{\eta P_{OUTEL}\tau_M}} = \sqrt{\frac{2\gamma_{STL}}{\eta\tau_M}} \quad (25)$$

This yields the result for the MMFS for an RLG:

$$\delta\omega_{RLG} = \sqrt{2\gamma_{STL} / \eta\tau_M} \quad (26)$$



Using this approach, we can now analyze the minimum measurable frequency shift of a laser (test laser: TL) when it is mixed with another laser (reference laser: RL) with much narrower spectral width (a delta function in the limiting case), as illustrated schematically in Figure 3. A simple extension of the analysis presented above shows that the spectral width of the beat signal can be expressed as:

$$\delta\mu = \sqrt{\frac{2D'}{\eta\tau_M}} = \sqrt{\frac{(\gamma_{STL-TL} + \gamma_{STL-RL})}{\eta\tau_M}} \quad (27)$$

If we consider the limiting case where  $\gamma_{STL-RL} \ll \gamma_{STL-TL}$ , we get the result for the MMSF for a laser using this approach (which we will denote as the standard technique) to be:

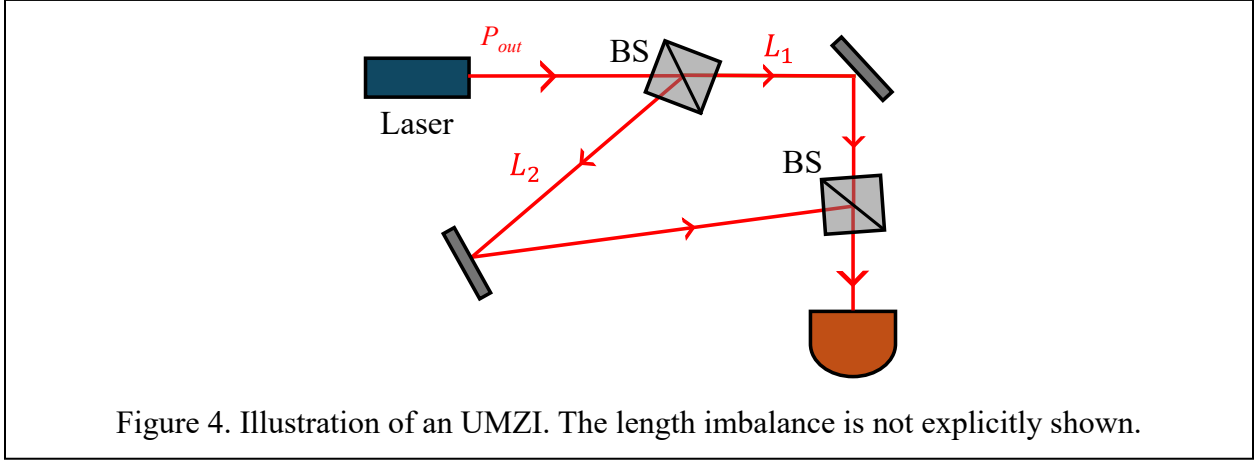


$$\delta\omega_{STD} \approx \sqrt{\gamma_{STL-TL}/\eta\tau_M} = \sqrt{\gamma_{STL-TL}\gamma_M/\eta} \quad (28)$$

which is the same as the result found in Eqn. (10) using Approach 1.

## 2. MMFS in a UMZI

Figure 4 shows a schematic of a UMZI, where the laser output is defined as  $P_{out}$  and the length



imbalance between two arms is  $\Delta L = L_2 - L_1$ . The time delay between the two paths can be expressed as  $\tau_{VAC} = \Delta L/c_0$ , where  $c_0$  is the vacuum speed of light. We consider the situation where the laser linewidth is limited by quantum noise only, we have shown in the main body [Eqn. \(17\)](#) that the output signal can be expressed as:

$$S = \frac{S_0}{2} + \frac{S_0}{2} e^{-\frac{\tau_{VAC}}{2\tau_{STL}}} \cos(\tau_{VAC}\Delta\omega) \quad (29)$$

where  $S_0$  is the maximum number of photons detected during measurement time  $\tau_M$  when constructive interference happens in a balanced MZI (corresponding to  $\tau_{VAC} = 0$ ) and  $\tau_{STL}$  is the inverse of the Schwalow-Townes linewidth (STL). Thus, the MMFS can be expressed as:

$$\delta\omega_{UMZI} = \left| \frac{\Delta S}{\partial S / \partial (\Delta\omega)} \right|_{\Delta\omega = \frac{\pi}{2\tau_{VAC}}} = \frac{\sqrt{S_0/2}}{\left| (S_0/2) \cdot (-\tau_{VAC}) \cdot \exp(-\tau_{VAC}/(2\tau_{STL})) \right|} \quad (30)$$

Defining  $x \equiv \tau_{VAC}/(2\tau_{STL})$ , Eq. (30) can be rewritten as:

$$\delta\omega_{UMZI} = \frac{1}{\sqrt{2S_0} e^{-x} x \cdot \tau_{STL}} = \frac{1}{\sqrt{2S_0} \cdot \tau_{STL}} \cdot \frac{e^x}{x} \quad (31)$$

The value of the MMFS diverge in the two extreme limits:  $\tau_{VAC} \rightarrow 0$  and  $\tau_{VAC} \gg \tau_{STL}$ . As such, there must be at least one specific value of  $x$  that minimizes the MMFS. By taking the derivative of Eq.(31) and making it equal to zero, we get:

$$\frac{d(\delta\omega_{UMZI})}{dx} = \frac{1}{\sqrt{2S_0} \cdot \tau_{STL}} \cdot \frac{d}{dx} \left( \frac{e^x}{x} \right) = \frac{1}{\sqrt{2S_0} \cdot \tau_{STL}} \cdot \left( \frac{e^x}{x} - \frac{e^x}{x^2} \right) = 0 \quad (32)$$

Solving Eq. (32) we get  $x = 1$ , which minimizes the MMFS in the UMZI:

$$\delta\omega_{UMZI} \big|_{\tau_{VAC}=2\tau_{STL}} = \frac{e}{\sqrt{2S_0} \tau_{STL}} \quad (33)$$

We recall that the STL can be written as:

$$\Gamma_{STL} = \frac{\Gamma_c}{2\langle n \rangle} = \frac{\Gamma_c \hbar\omega}{2P_{out} \tau_c} = \frac{\hbar\omega}{2P_{out} \tau_c^2} \quad (34)$$

where  $\langle n \rangle$  is the average number of photons coming out of the laser cavity,  $\Gamma_c = \tau_c^{-1}$  is the cavity decay rate,  $\hbar\omega$  is the single photon energy and  $P_{out}$  is the output power. In the standard case, the MMFS is the RMS of the STL and measurement bandwidth, i.e.,

$$\delta\omega_{STD} = \sqrt{\Gamma_{STL} / \tau_M} = \sqrt{\frac{\hbar\omega}{2P_{out} \tau_c^2 \tau_M}} \quad (35)$$

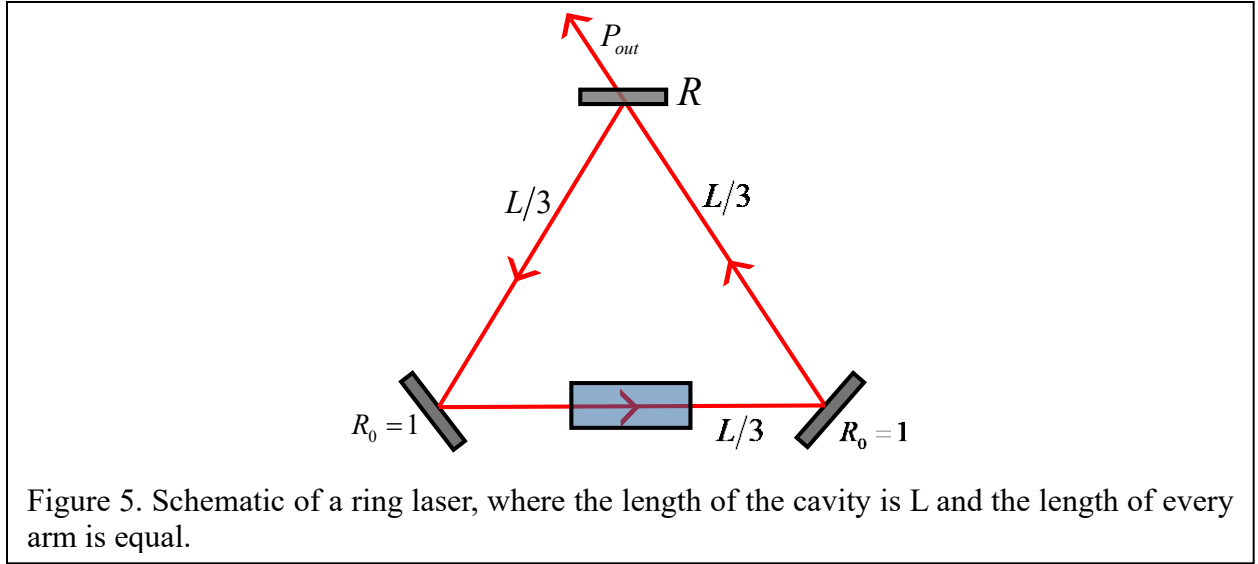
Therefore, the ratio of MMFSs in the UMZI and in the standard case can be written as:

$$\frac{\delta\omega_{UMZI}}{\delta\omega_{STD}} = \frac{e}{\sqrt{2S_0} \tau_{STL}} \cdot \left( \sqrt{\frac{\hbar\omega}{2P_{out} \tau_c^2 \tau_M}} \right)^{-1} = e \frac{\tau_c}{\tau_{STL}} \quad (36)$$

By using Eq. (34) and defining the number of photons coming out of the laser cavity per second as  $N_s = P_{out} / (\hbar\omega)$ , Eq.(36) can be simplified to

$$\frac{\delta\omega_{UMZI}}{\delta\omega_{STD}} = e \cdot \frac{\tau_c}{\tau_{STL}} = e \cdot \frac{\hbar\omega}{2P_{out} \tau_c} = \frac{e}{2N_s \tau_c} \ll 1 \quad (37)$$

since  $N_s \tau_c \gg 1$  in a laser. Therefore, even when no slow-light effect is present, the MMFS in an UMZI can potentially be much smaller than the MMFS in the standard case.



To estimate the value of the MMFSs, we consider an ideal ring laser, as shown in Figure 5, which has two mirrors with perfect reflectivities, and an output coupler with the intensity reflectivity defined as  $R$ . The cavity decay rate can be written as:

$$\Gamma_c \equiv \frac{1}{\tau_c} = \frac{c_0}{L} \cdot \frac{1-R}{\pi\sqrt{R}} \quad (38)$$

where  $\tau_c$  is the cavity decay time and  $L$  is the cavity length. We choose the wavelength to be 632.8 nm for specificity. Table 1 shows a list of parameters and the corresponding values of the MMFS.

$R$	$\lambda$ (nm)	$\tau_M$ (s)	$P_{out}$ (mW)	$L$ (cm)	$\frac{\Gamma_c}{2\pi}$ (MHz)	$\frac{\Gamma_{STL}}{2\pi}$ (mHz)	$\frac{\delta\omega_{STD}}{2\pi}$ (Hz)	$\frac{\delta\omega_{UMZI}}{2\pi}$ (nHz)
0.5	632.8	0.1	10	70	7.7	5.8	0.24	0.50
0.8					2.4	0.58	0.076	0.050
0.9					1.1	0.13	0.036	0.011
0.95					0.56	0.031	0.018	0.0026

Table 1. The calculated MMFSs for different values of  $R$ , the output coupler reflectivity. Here,  $\lambda$  is the laser wavelength,  $\tau_M$  is the measurement time,  $P_{out}$  is the output power of the laser and  $L$  is the length of the ring cavity.  $\Gamma_c$  is the calculated cavity decay rate and  $\Gamma_{STL}$  is the Schawlow-Townes Linewidth.

The fundamental principle of quantum mechanics requires  $\delta\omega \cdot \delta t \geq 1$ , where  $\delta t$  is the measurement time  $\tau_M$ . Therefore, we can write

$$\begin{aligned}\delta\omega_{STD} \cdot \delta\tau &\geq 1 \Rightarrow \delta\omega_{STD} \cdot \tau_M^{STD} \geq 1 \\ \delta\omega_{UMZI} \cdot \delta\tau &\geq 1 \Rightarrow \delta\omega_{UMZI} \cdot \tau_M^{UMZI} \geq 1\end{aligned}\quad (39)$$

By only considering the lower bound in Eq. (39) and utilizing Eq. (33) and Eq. (35), we can get

$$\begin{aligned}\delta\omega_{STD} \cdot \tau_M^{STD} &= 1 \Rightarrow \sqrt{\frac{\Gamma_{STL}}{\tau_m}} \cdot \tau_M^{STD} = 1 \Rightarrow \tau_M^{STD} = \Gamma_{STL}^{-1} = \tau_{STL} \\ \delta\omega_{UMZI} \cdot \tau_M^{UMZI} &= 1 \Rightarrow \frac{e}{\sqrt{2N\tau_m \cdot \tau_{STL}}} \cdot \tau_M^{UMZI} = 1 \Rightarrow \tau_M^{UMZI} = \frac{2N \cdot \tau_{STL}^2}{e^2}\end{aligned}\quad (40)$$

Therefore, the MMFS sets a lower bound on the measurement time. Assuming the same  $R$ ,  $\lambda$ ,  $P_{out}$  and  $L$  as given in Table 1,  $\tau_M^{STD}$  and  $\tau_M^{UMZI}$  can be obtained by Eq. (40) and Table 2 shows the results as well as the ratio between these two measurement time. It's worth noting that the ratio of the measurement time is inversely proportional to the square of the corresponding MMFS, which is expected numerically.

$R$	$\lambda$ (nm)	$P_{out}$ (mW)	$L$ (cm)	$\tau_M^{STL}$ (sec)	$\tau_M^{UMZI}$ (*10 <sup>20</sup> sec)	$\frac{\tau_M^{UMZI}}{\tau_M^{STL}}$
0.5	632.8	10	70	27.33	0.0643	2.4*10 <sup>17</sup>
0.8				273.3	6.43	2.3*10 <sup>18</sup>
0.9				1230	130	1.1*10 <sup>19</sup>
0.95				5194	2320	4.5*10 <sup>19</sup>

Table 2. Calculated measurement time using quantum limit.

In our experiment, without the presence of slow-light medium and having a length imbalance of 0.52 meters, the MMFS is determined to be 38 kHz when the measurement time is 0.3 sec. Thus, we can calculate  $\delta\omega_{UMZI} \cdot \delta t = 38\text{kHz} \cdot 0.3\text{sec} = 11400 \gg 1$ . Meanwhile, at the group index 1752, which is the highest group index that has been achieved in our cases, the MMFS is measured to be 104 Hz, which gives  $\delta\omega_{UMZI} \cdot \delta t = 104\text{Hz} \cdot 0.3\text{sec} \approx 30 \gg 1$ .

<sup>1</sup> T.A. Dorschner, H.A. Haus, M. Holz, I.W. Smith, H. Statz, "Laser gyro at quantum limit", IEEE J. Quant. Elect. QE-16, 1376 (1980)

<sup>2</sup> B. T. King, "Application of superresolution techniques to RLGs: exploring the quantum limit," Applied Optics **39**, 6151 (2000)

<sup>3</sup> W. W. Chow, J. Gea-Banacloche, L. M. Pedrotti, V. E. Sanders, W. Schleich, and M. O. Scully, "The Ring Laser Gyro," Review of Modern Physics, Vol. 57, No. 1, p. 61 (1985)

## Supplement II: Noise Analysis in UMZI

In the main body of the paper, we have demonstrated improvement of the minimum measurable frequency shift (MMFS) by implementing the SLAUMZI. We have also shown that the demonstrated MMFS was larger than the theoretically predicted value because of noise in excess of the shot-noise. Here, we describe details of a comprehensive analysis of the noise in the SLAUMZI system, and propose techniques that can be used for further improvement. The rest of this supplement is organized as follows. In Section 1, we present theoretical and experimental studies of white noise, because of its equivalence to shot-noise. The formalism developed in this section is used in the subsequent sections when addressing shot noise. In Section 2, we present results of measuring the shot noise of light directly from a laser by using avalanche photo diode (APD). In Section 3, we present results of measuring shot-noise at the output of one port of the unbalanced Mach-Zehnder interferometer (UMZI), and demonstrate that the interference present in the UMZI does not add excess noise. In Section 4, we show that when the probe laser is offset phase locked to the pump laser, a significant amount of excess noise is produced. In Section 5, we show how a subtraction technique can potentially be used to suppress the effect of excess intensity noise.

### 1. Simulation and measurement of the spectral density of white noise

Figure 1(a) shows the schematic used to measure the spectral density of white noise, which is generated by a function generator. The DC blocker (Mini-Circuits, BLK-89-S+), which in practice is a bandpass filter, passes signals ranging from 0.1 MHz to 8000 MHz. The bandwidth of the amplifier (Mini-Circuits, ZFL-500LN+) covers 0.1 MHz to 500 MHz, with a nominal amplification factor of 24 dB, denoted as  $g$ . The output of the amplifier, denoted as  $S_A$ , is mixed with an RF signal, denoted as  $S_R$ , which is at 500 kHz. The bandwidth of the frequency mixer (Mini-Circuits, ZAD-6+) covers 3 kHz to 100 MHz. The output of the mixer, denoted as  $S_M$ , is passed through a low-pass filter (LPF) with a cutoff-frequency far below that of the RF signal. The inverse of the bandwidth of the LPF represents the integration time. As such, the components shown within the dashed red lines acts effectively as a spectrum analyzer.

Figure 1(b) shows the power spectral density of the white noise, measured directly by connecting the function generator to a conventional spectrum analyzer (Signal Hound, SA44B). As can be seen in Figure 1(b), the bandwidth of the white noise, defined as the -3dB point, is 7 MHz. Therefore, the bandwidths of the DC blocker and the amplifier cover the whole spectrum of the white noise except a small range of low frequencies (DC to 0.1 MHz), which has very little effect on the measurement, since the frequency of the RF signal is not in this range.

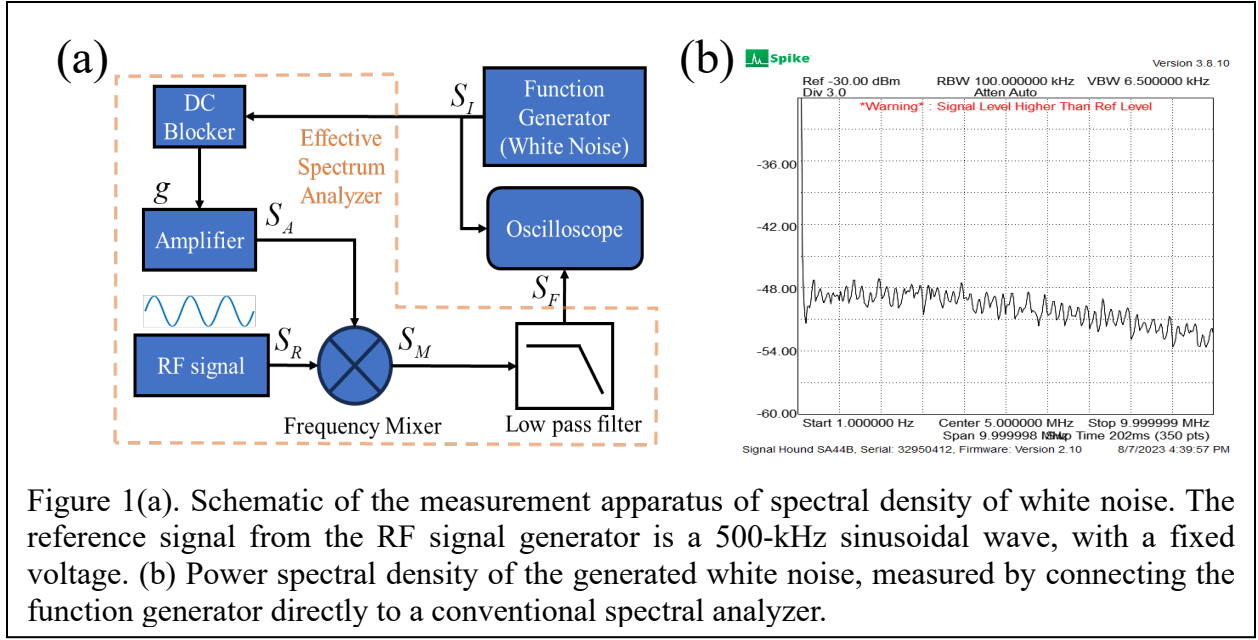


Figure 1(a). Schematic of the measurement apparatus of spectral density of white noise. The reference signal from the RF signal generator is a 500-kHz sinusoidal wave, with a fixed voltage. (b) Power spectral density of the generated white noise, measured by connecting the function generator directly to a conventional spectral analyzer.

The white noise in general can be expressed as a sum over a set of sinusoidal waves where the frequency and the phase of each sine wave is chosen randomly with a uniform density [1]. Therefore, the white noise can be written as:

$$S_I = \sum_{k=1}^m \frac{\sqrt{2}A_0}{\sqrt{m}} \sin(\omega_k t + \varphi_k) \quad (1)$$

where  $A_0$  is the root-mean-square (RMS) value of the signal, which is in unit of voltage in this case, and  $m$  is the number of sine waves present in the white noise. Because the white noise averages to zero, the RMS value is equivalent to the standard deviation (STD). Therefore, the STD is used in all discussions to follow for characterizing the noise level.

It is important to verify that the definition of  $A_0$  and Eq. (1) represent the white noise properly. The white noise is set to different STD voltages in the function generator and is directly sent to both the DC blocker and the high input impedance (1 Mega-Ohm) oscilloscope, where the experimentally determined STD voltages are calculated from the data read from the oscilloscope. It should be noted here that the bandwidth of the oscilloscope (200 MHz) is far above the bandwidth of the white noise (7 MHz), which guarantees the fidelity of the white noise. Define the STD voltage set in the function generator as  $V_{STD}^{set}$  and the STD voltage measured from the oscilloscope as  $V_{STD}^{exp}$ . Figure 2(a) compares these two voltages defined above. The ratio between the experimentally measured values and the ideal values of the STD remains a constant ( $\sim 0.73$ ). As such, the difference between the measured and ideal values is attributable to the fact that the signal is loaded down by the DC blocker, which has a low input impedance. In the following analysis, unless stated explicitly to be otherwise,  $V_{STD}^{exp}$  is used in all simulations.

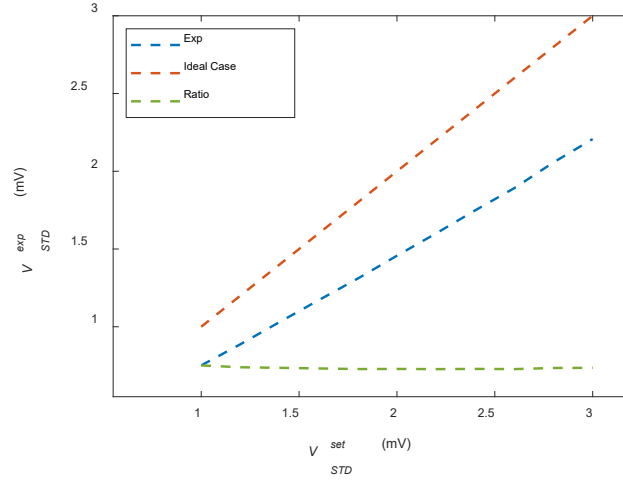


Figure 2. Comparison between  $V_{STD}^{set}$  and  $V_{STD}^{exp}$ . To calculate  $V_{STD}^{exp}$ , 7000 data points are taken from the oscilloscope with a sampling rate of 1 MSample/s and a sampling time of 7 ms. The red dashed line represents the ideal case. The blue line denotes the experimental measurement. The green line shows the ratio between the experimental values and the ideal value. See text for details.

To model the white noise, we set  $A_0$  to  $V_{STD}^{exp}$  and use Eq. (1). The corresponding STD is plotted along with the experimentally measured STD in Figure 3. It can be seen that the STD of constructed white noise is close enough to the experimental one, confirming the validity of using Eq. (1) to model the white noise.

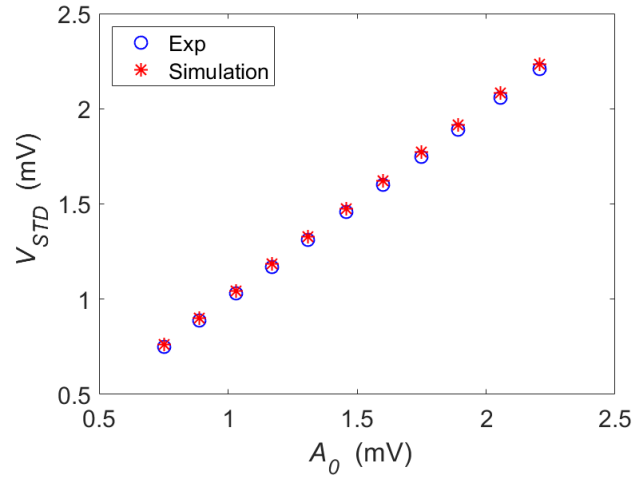


Figure 3. The STD of the simulated white noise compared with the experimentally measured one. Here  $A_0$  is made to equal to  $V_{STD}^{exp}$ .

In the simulation,  $\omega_k$  is chosen in a random process where  $f_0 = B_w / m$  is the fundamental frequency and  $B_w$  is the bandwidth of the white noise. We tested that the spectral density is a constant within  $B_w$ . At the same time,  $\varphi_k$  is chosen randomly  $m$  times from  $(0, 2\pi]$  by a Poisson point experiment. In choosing the value of  $m$ , we ensure that  $m \gg B_w / B_c$  where  $B_c$  is the bandwidth of the LPF. The specific value we chose to use is  $m = 5 \times 10^4$ .

If we assume that all frequencies below 100kHz are blocked by the DC blocker, after amplification, the output signal from the amplifier becomes:

$$S_A \equiv gS_I = \sum_{k=1}^m g \frac{\sqrt{2}V_{STD}^{\exp}}{\sqrt{m}} \sin(\omega_k t + \varphi_k). \quad (2)$$

The reference signal, which is mixed with the amplified signal, can be expressed as:

$$S_R \equiv V_R \sin(\omega_R t + \varphi_R), \quad (3)$$

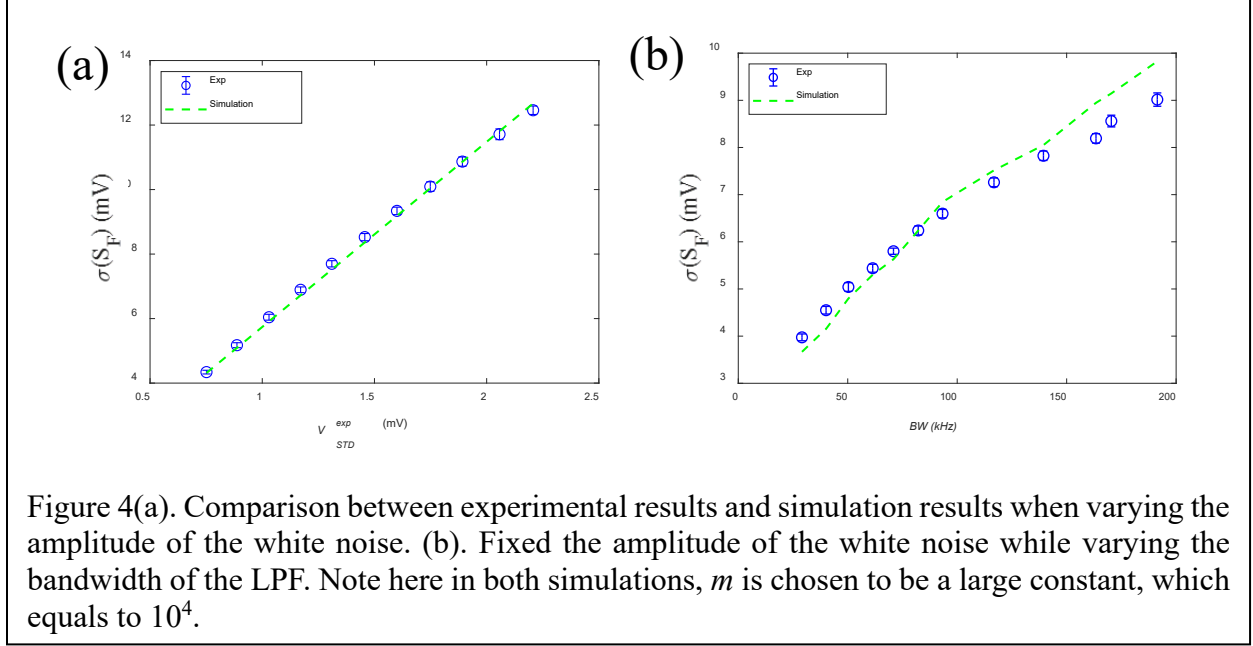
where  $V_R$  is in unit of voltage and  $\varphi_R$  is the phase of the signal, and  $\omega_R$  is the frequency of the reference signal. We can then express the output of the frequency mixer as:

$$\begin{aligned} S_M &\equiv S_A * S_R / V_{nor} = \sum_{k=1}^m g \frac{\sqrt{2}V_{STD}^{\exp}V_R}{V_{nor}\sqrt{m}} \sin(\omega_k t + \varphi_k) \sin(\omega_R t + \varphi_R) \\ &= g \frac{\sqrt{2}V_{STD}^{\exp}V_R}{V_{nor}\sqrt{m}} \sum_{k=1}^m \left( \cos[(\omega_k - \omega_R)t + \varphi_k - \varphi_R] - \cos[(\omega_k + \omega_R)t + \varphi_k + \varphi_R] \right). \end{aligned} \quad (4)$$

where here  $V_{nor}$  is a scaling factor dictated by the mixer, which was determined experimentally to be  $\sim 0.66$  Volt. The signal after the LPF can be written as:

$$S_F = g \frac{\sqrt{2}V_{STD}^{\exp}V_R}{V_{nor}\sqrt{m}} \sum_{|\omega_k - \omega_R| < B_c} \cos[(\omega_k - \omega_R)t + \varphi_k]. \quad (5)$$

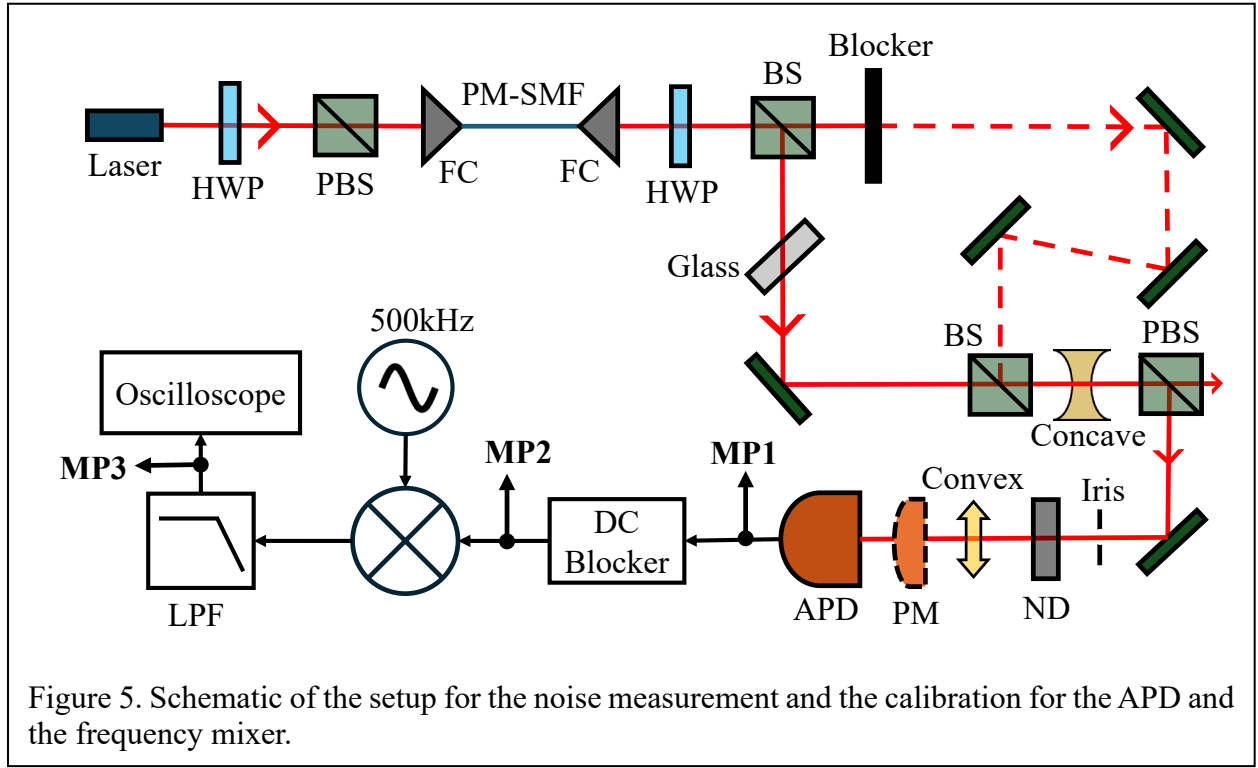




We implemented the experiment using the white noise generated from the function generator. In Figure 4(a) and (b), we show (the blue circles) the standard deviation of the signal observed at the output of the effective spectrum analyzer shown in Figure 1(a), as functions of the standard deviation of the white noise and the bandwidth of the LPF, respectively. The simulation result obtained from Eq. (5) are shown as the dashed lines. As can be seen, the agreement between the experimental results and the simulations is quite reasonable.

## 2. Measurement of Shot Noise using an Avalanche Photo Diode

In the main body of the paper, we described how the signals for the UMZI and the SLAUMZI were measured using an avalanche photo diode (APD). Here, we describe how we observed measurement of shot noise using the APD while blocking one arm of the MZI, as shown in Figure 5. The output of the APD is connected to the input of an effective spectrum analyzer, similar to the one shown in Figure 1(a), but without the amplifier. A 4-channel oscilloscope is connected to three monitoring points (denoted as MP1, MP2, and MP3). Here, MP1 and MP2 monitor the DC and the AC outputs of the APD, respectively, and MP3 monitors the output of the effective spectrum analyzer.



When excess noise is negligible compared to photon shot noise, the average voltage (denoted as the DC voltage) on the APD can be expressed as:

$$V_{DC} = kP = kN\hbar\omega, \quad (6)$$

where  $P$  is the optical power,  $k$  is the conversion coefficient that has a unit of Volt/Watt,  $N$  is the number of photons per sec, and  $\omega$  is the frequency. During a time window  $\tau$ , the energy uncertainty is  $\Delta E = \sqrt{N\tau}\hbar\omega$ , so that power uncertainty can be expressed as:

$$\Delta P = \frac{\Delta E}{\tau} = \hbar\omega\sqrt{\frac{N}{\tau}}. \quad (7)$$

The uncertainty in the output voltage of the APD can be written as:

$$\Delta V = k\Delta P = k\hbar\omega\sqrt{\frac{N}{\tau}} = \sqrt{\frac{k\hbar\omega}{\tau}}\sqrt{V_{DC}}. \quad (8)$$

The value of the parameter  $k$  for the APD can be determined experimentally. When excess noise is taken into account, the uncertainty in the signal can be expressed as:

$$\Delta V = \sqrt{\frac{k\hbar\omega}{\tau}}\sqrt{V_{DC}} + C_{exc}, \quad (9)$$

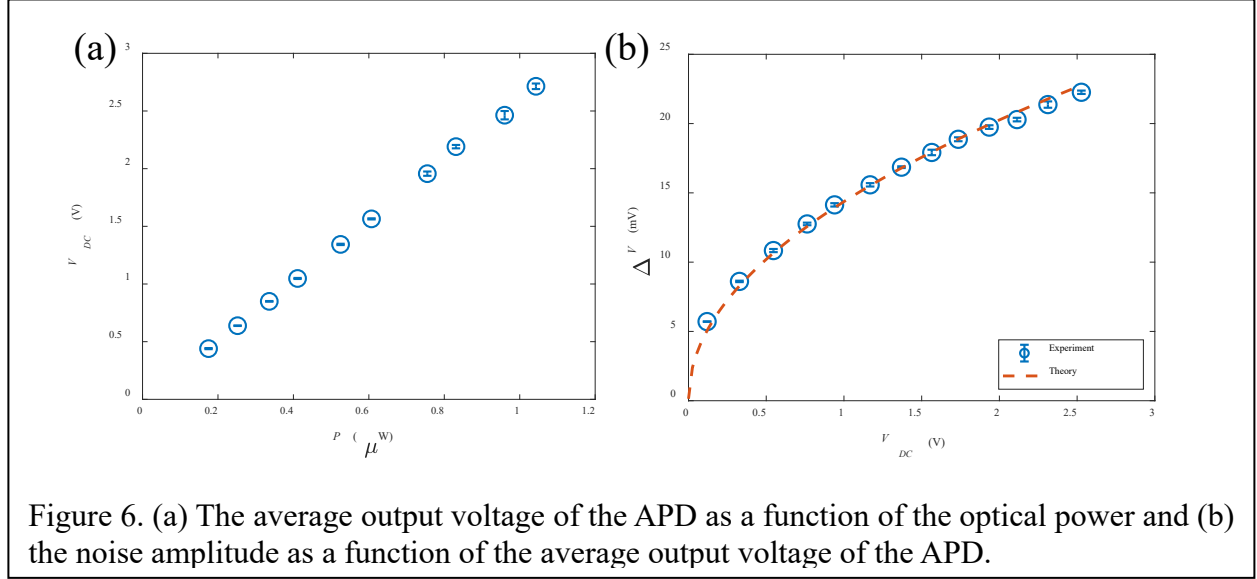


Figure 6. (a) The average output voltage of the APD as a function of the optical power and (b) the noise amplitude as a function of the average output voltage of the APD.

where  $C_{exc}$  represents the noise in the absence of any light. The mean value of this excess noise was found to be vanishingly small experimentally.

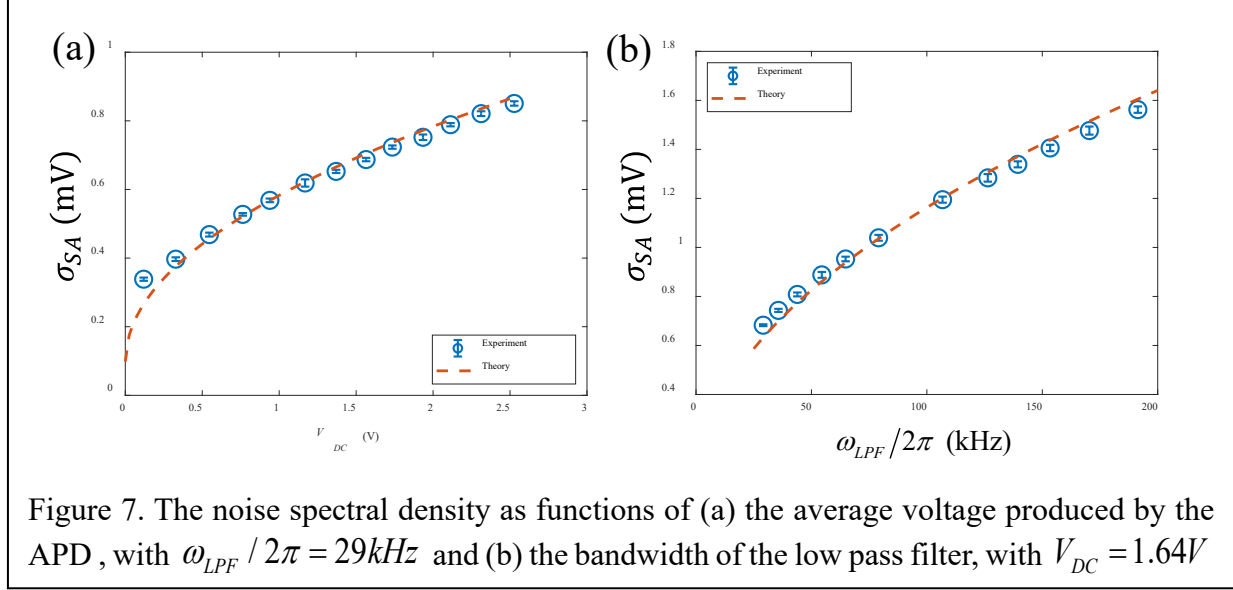
In Figure 6(a), we show the average voltage as a function of the incident light power, which was measured by inserting a power meter in front of the APD and then removed. From this data, the coefficient  $k$  is calculated to be  $2.58 \times 10^6$  V/W, which agrees well with the specification provided by the manufacturer. Figure 6(b) plots the noise amplitude as a function of the average voltage, shown as circles with error bars, along with the theoretical prediction, shown as the dashed trace. In order to find  $C_{exc}$ , we minimized the mean square of the difference between the experimental values and theoretical values of  $\Delta V$ , yielding  $C_{exc} \approx 0.14$  mV.

The standard deviation (SD) of the output of the spectrum analyzer can be expressed as:

$$\sigma_{SA} = \sqrt{\frac{2\omega_{LPF}}{\omega_{APD}}} * \sqrt{\frac{k\hbar\omega}{\tau_{APD}}} * \sqrt{V_{DC}} + C_{sd} \quad (10)$$

where  $\omega_{LPF}$  and  $\omega_{APD} (= 1/\tau_{APD})$  are the bandwidths of the LPF and the APD, respectively. The offset  $C_{sd}$  represents the SD of the excess noise present in the absence of any input light. Since  $C_{sd}$  is very small, we have made the simplifying assumption that the SD of the excess noise is independent of the value of the  $\omega_{LPF}$ . Figure 7 shows  $\sigma_{SA}$  functions of the average voltage and  $\omega_{LPF}$ , which represent the measurement bandwidth. By fitting the experimental data to Eq.(10),  $C_{sd}$  is determined to be 0.1 mV and 0.01 mV in Figure 7(a) and Figure 7(b), respectively. The reason for the discrepancy in the value of  $C_{sd}$  determined from these two sets of data may be attributable to the uncertainties in the values of  $\omega_{LPF}$ , which was inferred from the markings on the potentiometer used for tuning the LPF. However, when this experiment was repeated after unblocking the other arm of the UMZI, the value of  $C_{sd}$  was found to be 0.1 mV for both cases.

Thus, the value of  $C_{sd}$  extrapolated from the plots of  $\sigma_{SA}$  versus  $\omega_{LPF}$  changed from 0.01 mV in this case to 0.1 mV in the case when the other arm of the UMZI was unblocked. This is consistent with the idea that these variations in the values of  $C_{sd}$  is due to uncertainties in the values of  $\omega_{LPF}$ .



### 3. Noise measurement in an UMZI

We describe now the noise properties of the output of an unbalanced MZI (UMZI) without any slow-light effect, by removing the blocker in Figure 5. We keep the laser power incident on the input BS of the UMZI unchanged, and vary the angular position of the glass plate in one arm of the MZI to change the amount of light exiting the detection port of the output BS of the UMZI.

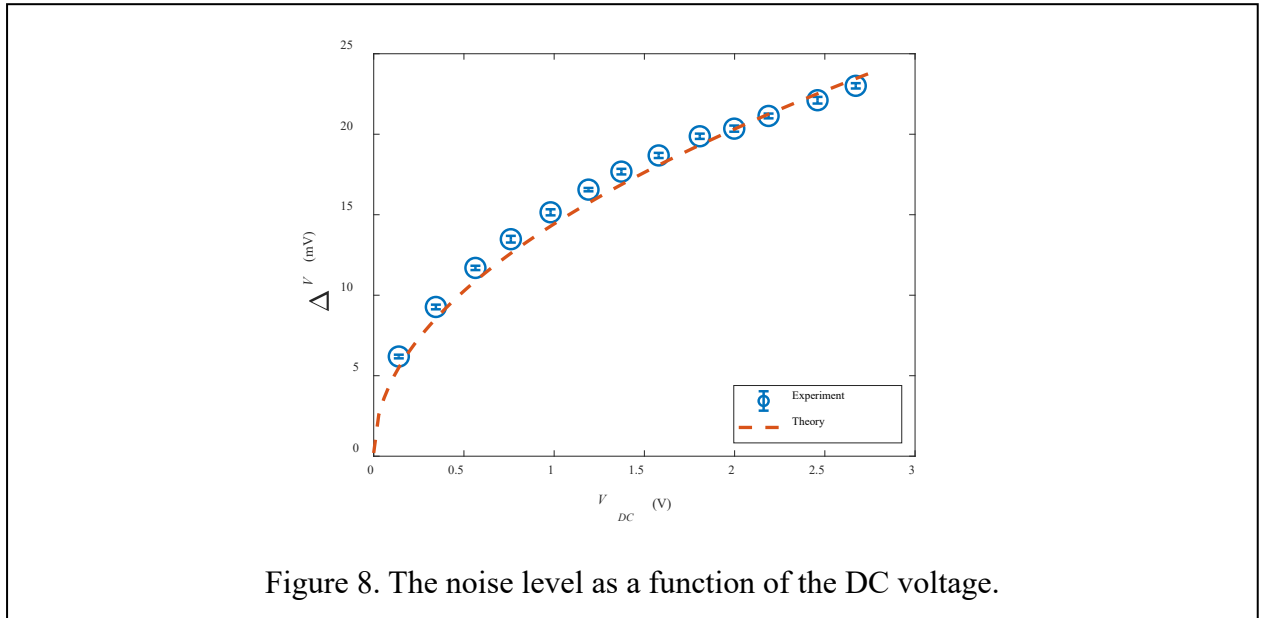


Figure 8. The noise level as a function of the DC voltage.

Figure 8 shows the noise amplitude as a function of the average voltage, observed at the MP2 port, and the corresponding theoretical values predicted by Eq. (9). Here  $C_{exc}$  is determined to be 0.2 mV, which is close to the value of the same found when one arm of the UMZI was blocked. This indicates that any excess noise attributable to fluctuations in the relative phase between the two arms of the UMZI is negligible. The standard deviations of the signal at the output of the effective spectrum analyzer, observed at the MP3 port, are shown in Figure 9, as functions of the average voltage and the measurement bandwidth (i.e.,  $\omega_{LPF}$ ), along with predictions made by Eq.(10). The value of  $C_{sd}$  was determined by a fitting process, and were found to be 0.1 mV in both cases.

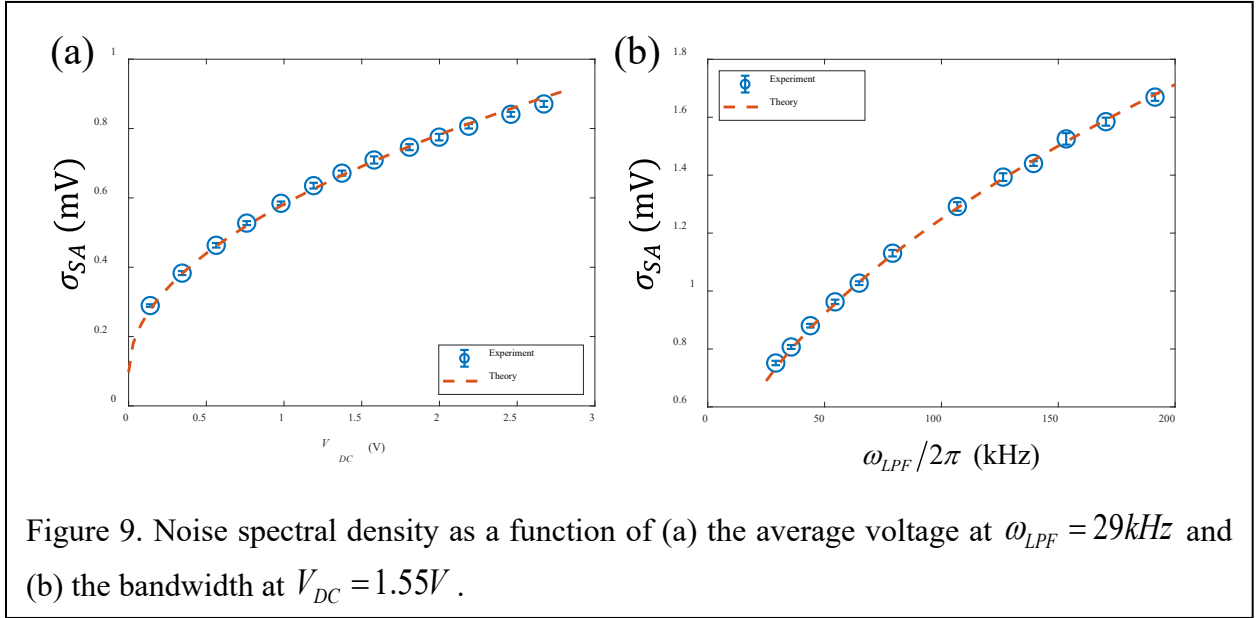


Figure 9. Noise spectral density as a function of (a) the average voltage at  $\omega_{LPF} = 29\text{kHz}$  and (b) the bandwidth at  $V_{DC} = 1.55\text{V}$ .

#### 4. Noise measurement in an UMZI using an offset phase locked laser

For implementing the SLAUMZI, we used Electromagnetic Induced Transparency (EIT) for generating the slow-light effect. The EIT process required the use of two lasers: the probe and the pump. The probe laser was made phase-coherent with the pump laser using an offset phase lock (OPL) system, as described in the main body of the paper. Unfortunately, the OPL system is not perfect, and introduces excess noise in the SLAUMZI apparatus. Here, we describe a study of this excess noise, using the UMZI without the slow light effect.

Figure 10 shows the schematic of the setup used for this study. The Probe laser is locked to the Pump laser by the OPL system with a frequency difference corresponding to the hyperfine splitting between  $5S_{1/2}, F=2$  and  $5S_{1/2}, F=3$  in  $\text{Rb}^{85}$ , which is 3.0357GHz. The OPL has two inputs: one is the beatnote between the two lasers obtained from the fiber-coupled photodetector (PD1), and the other is the radio frequency signal from the frequency synthesizer, which is tuned to 3.0357GHz. The Pump laser is separately locked to the resonance frequency of the  $5S_{1/2}, F=2$

to  $5P_{1/2}, F'=3$  transition by a laser locking box (Moku Lab, Liquid Instrument). During the SLAMUZI experiment, both pump and probe lasers enter the UMZI. However, for the study described below, only the probe laser enters the UMZI

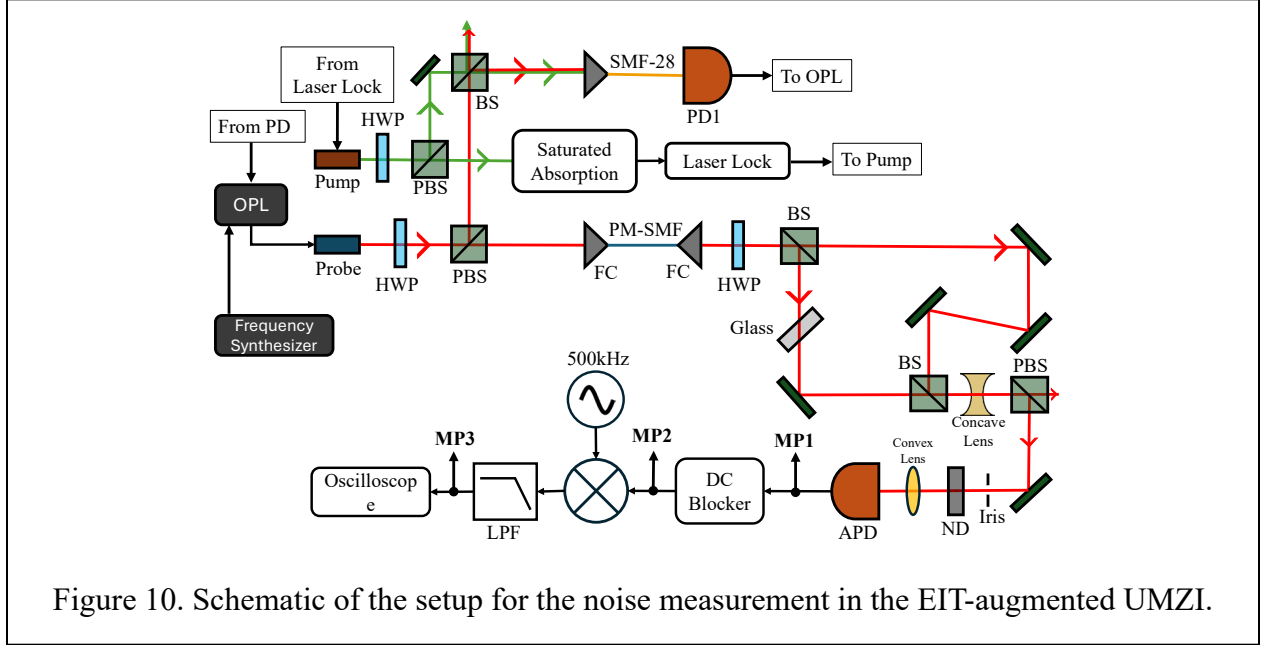
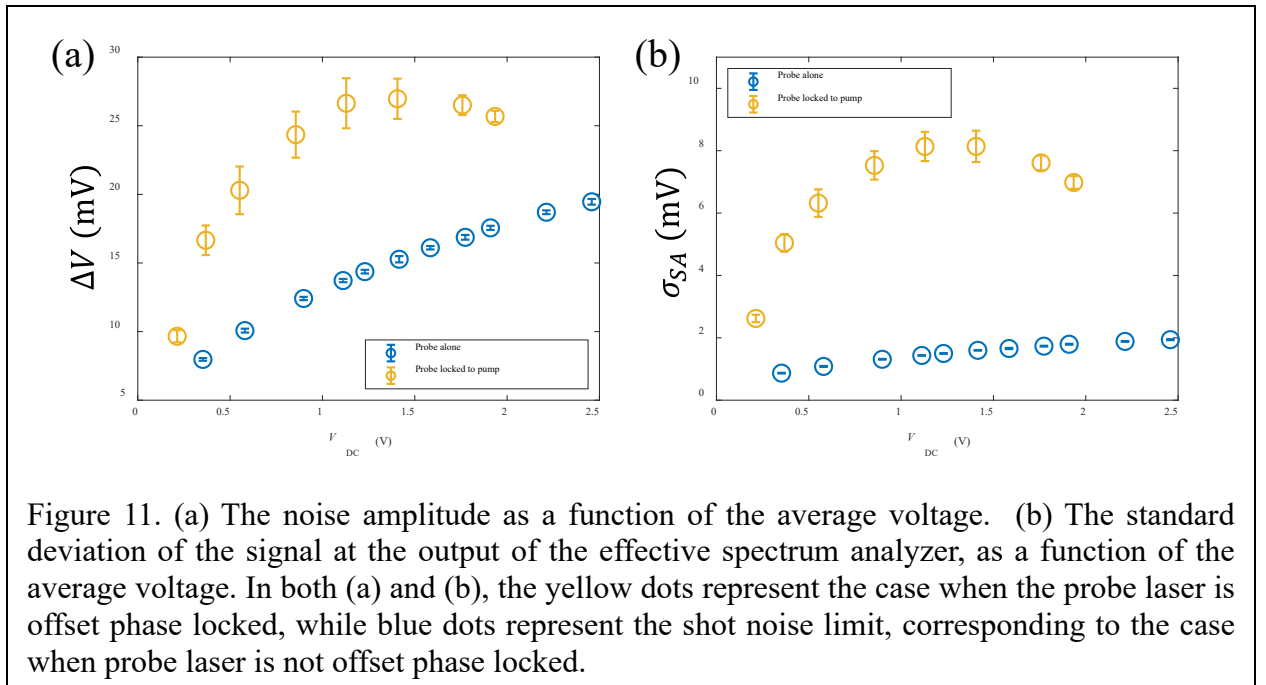


Figure 11 shows the noise amplitude (monitored at MP2) and the standard deviation of the output of the effective spectrum analyzer (monitored at MP3) as functions of the average voltage. Previous experiment data (shown as the blue circles) where independent probe laser is used in the



UMZI is plotted as a reference. It is obvious that when the probe laser is offset phase locked, the standard deviation is no longer shot noise limited.

A commercial spectrum analyzer (SB44B, Signal Hound) was used to qualitatively analyze the noise in the frequency domain. Figure 12 shows the spectral density of the noise observed at the output of the effective spectrum analyzer (i.e., at the MP3 port) for different average voltages produced by the APD at the MP2 port. The center frequency is 1 MHz and the span is 2 MHz for every subset in Figure 12, so that the signal ranges from 1 Hz to 2 MHz. The value of the bandwidth (RBW) and the video bandwidth (VBW) are 30 kHz and 6.5 kHz, respectively. For small average voltages, the spectral density of the noise shows good uniformity across the whole 2 MHz span, which is consistent with shot noise. However, as the average voltage increases, the spectral density of the noise surges at lower frequencies (<1 MHz) while remaining relatively flat at higher frequencies. This implies that use of the OPL process produces a strong low-frequency component of excess noise that is much larger than the shot noise.

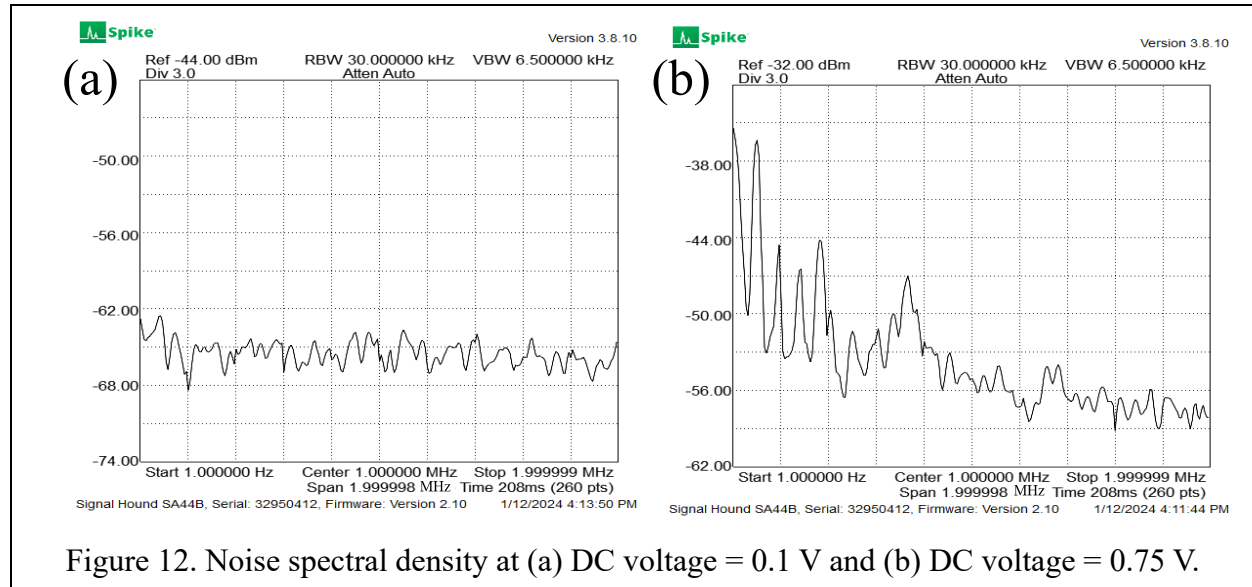
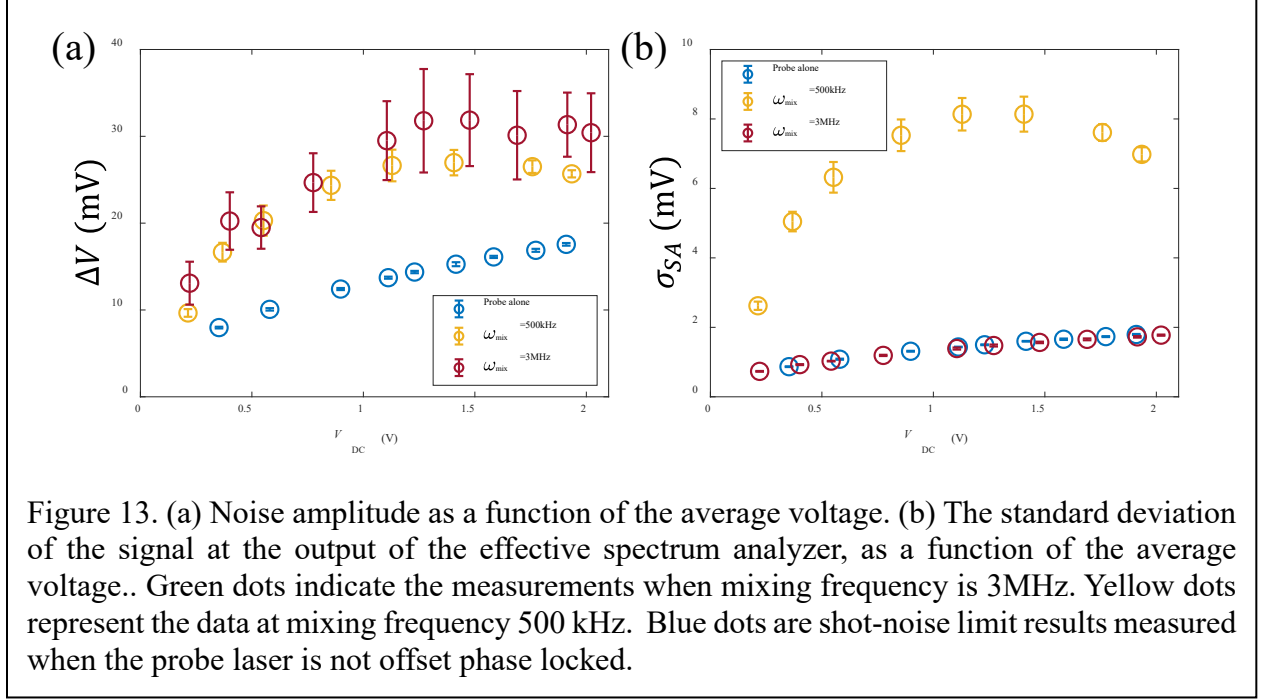


Figure 12. Noise spectral density at (a) DC voltage = 0.1 V and (b) DC voltage = 0.75 V.

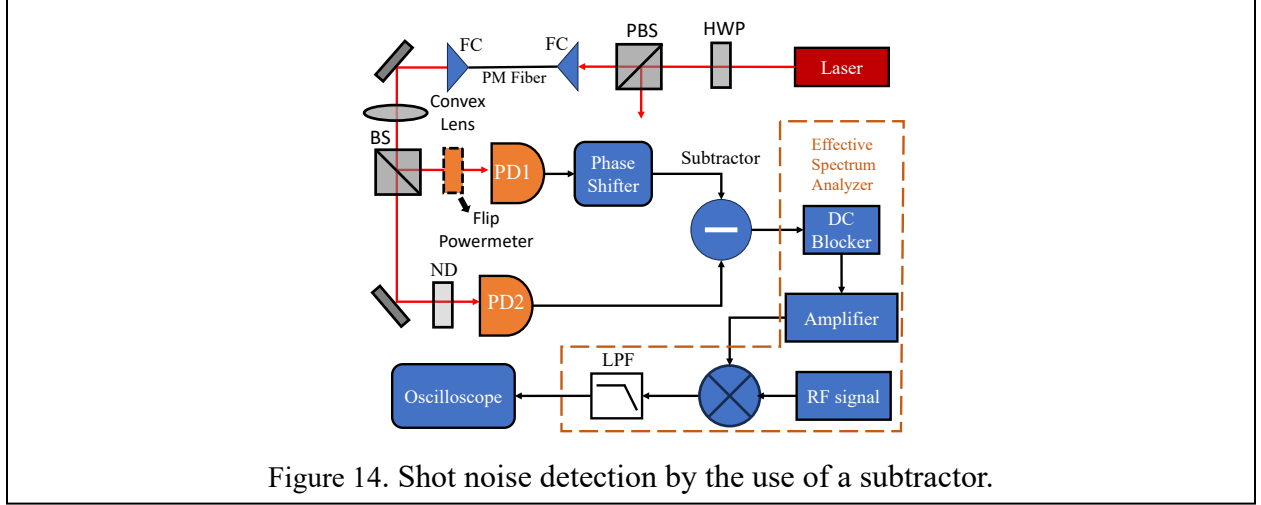
In order to suppress the effect of this low-frequency noise, we change the RF frequency, used of mixing with the signal, from 500 kHz to 3 MHz in the effective spectrum analyzer. Figure 13 illustrates the noise detected by the APD at the MP2 port, and the standard deviation of the signal observed at the output of the effective spectrum analyzer (i.e., at the MP3 port) as a function of the average voltage. For comparison, data with the 500 kHz mixing frequency (blue circles) and data without offset phase lock (red circles) are also presented. As can be seen, the standard deviation of the signal at the output of the effective spectrum analyzer follows the shot noise limit very well for the 3 MHz mixing frequency.



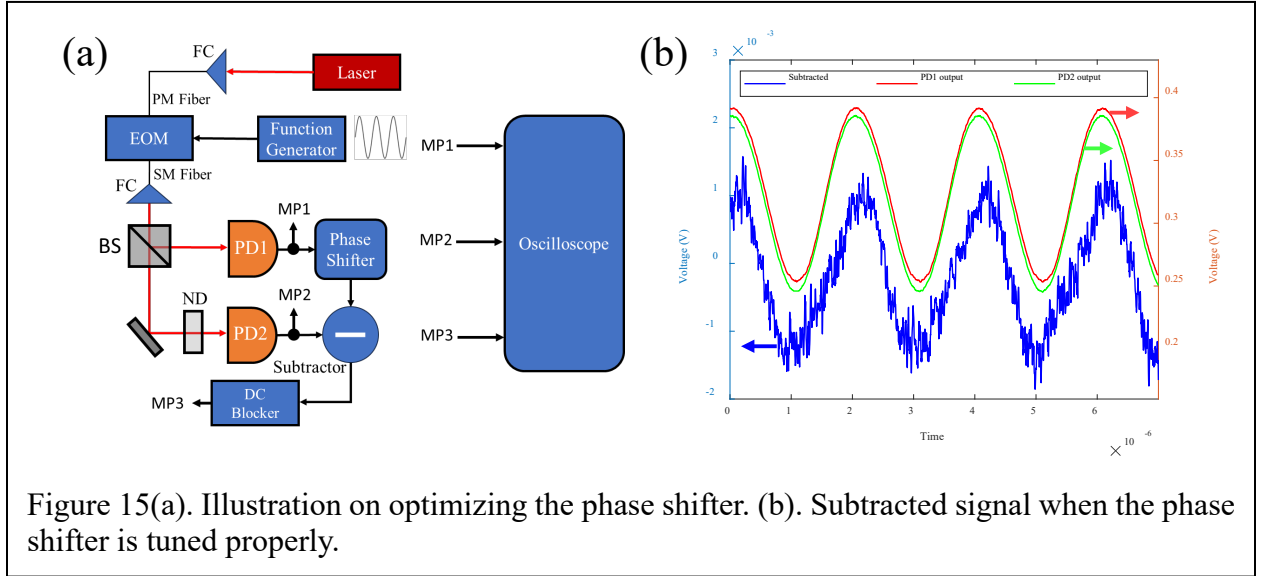
## 5. Balanced Detection for Suppressing the Effect of Excess Noise

As we have shown above, in some situations the intensity noise in a laser beam can be larger than the shot noise. To make the measurement shot-noise-limited, we have investigated the use of a homodyne scheme to suppress the intensity noise, as illustrated in Figure 14(a). The beam from an external-cavity diode laser is passed through a polarization-maintaining (PM) fiber. The power coupled into the fiber can be varied by the combination of the halfwave plate (HWP) and the polarizing beam splitter (PBS). A convex lens is used to make the beam size smaller than the active areas of photodetectors. A 50:50 beam splitter (BS) splits the beam into two parts with equal power and a neutral density filter (ND) is inserted to equalize the intensities in the two paths. Due to some difference in the the frequency responses of the two photodetectors (PDs), we inserted a phase-shifter after the output of one of the detectors (PD1). The phase-shifter has a bandwidth of 30 MHz, and does not attenuate the signal, within its bandwidth. A subtractor with a bandwidth of 30 MHz is used to produce the difference between the signal from PD2 and the output of the phase-shifter. The subtracted signal goes through an effective spectrum analyzer similar to the one shown earlier in Figure 1(a), and is displayed on the oscilloscope. The frequency of the RF signal fed to the mixer is 500 kHz. The amplifier shown in the effective spectrum analyzer is composed of two amplifiers (Mini-Circuit, ZFL-500LN+ and ZFL-500) in series. The LPF has a cutoff frequency tunable from 29 kHz to 191 kHz.





In order to optimize the subtraction process, we carried out a calibration process, as illustrated in Figure 15(a). The laser beam was directed into an electro-optic modulator (EOM) through fiber coupling. The EOM was driven by a function generator to produce a sinusoidal intensity modulation. The outputs from the two PDs were monitored along with the subtracted signal. It was determined that when the shift produced by the phase-shifter is minimal, the peak-to-peak (PTP) value of the subtracted signal was  $\sim 23$  mV. We tuned the phase-shifter to minimize this PTP value to  $\sim 2.3$  mV, as shown in Figure 15(b). The EOM was then removed, and this setting for the phase-shifter was used for demonstrating suppression of excess noise.



It is reasonable to assume that the shot noise has the same form as the white noise. As such, we can express the shot noise as:

$$S_{SN} = \sum_{k=1}^m \frac{\sqrt{2}V_{STD}}{\sqrt{m}} \sin(\omega_k t + \varphi_k) \quad (11)$$

Here, the standard deviation is related to the parameters of the experiment as follows:

$$V_{STD} = \sqrt{\alpha R \hbar \omega / \tau} \sqrt{V_0} \quad (12)$$

where, for each detector, which are essentially identical,  $R$  (volts/amp) is the transimpedance gain,  $\alpha$  (amp/watt) is the responsivity,  $\tau$  is the inverse of the bandwidth, and  $V_0$  (volts) is the DC output. Therefore, the shot noise at the output of the amplifiers can be expressed as:

$$S_A \equiv g_{tot} S_I = \sum_{k=1}^m g_{tot} \frac{\sqrt{2} V_{STD}}{\sqrt{m}} \sin(\omega_k t + \varphi_k) \quad (13)$$

where the value of the amplifier gain was determined to be  $\sim 393$ . The shot noise at the output of the LPF can be written as:

$$\begin{aligned} S_F &= g_{tot} \beta \frac{\sqrt{2} V_{STD}}{\sqrt{m}} \sum_{|\omega_k - \omega_R| < B_c} \cos[(\omega_k - \omega_R)t + \varphi_k] \\ &= g_{tot} \beta \sqrt{\frac{2\alpha R \hbar \omega}{\tau m}} \sqrt{V_0} \sum_{|\omega_k - \omega_R| < B_c} \cos[(\omega_k - \omega_R)t + \varphi_k] \end{aligned} \quad (14)$$

where  $\omega_R = 500 \text{ kHz}$  is the mixing frequency,  $B_c = 191 \text{ kHz}$  is the bandwidth of the LPF, and the value of  $\beta$  was determined to be  $\sim 0.89$  by calibrating the frequency mixer.

It is important to notice that Eq.(14) is the theoretical expression of the shot-noise limited signal displayed on the oscilloscope. Therefore, the standard deviation of this signal must be calculated and used to compare with experimental results. When the number of sine waves  $m$  is large enough, the standard deviation of Eq.(14) can be written as:

$$\sigma(S_F) = C_0 \sqrt{V_0} \quad (15)$$

where  $C_0$  is a unitless constant and can be determined by simulation. In practice, we choose  $m = 5 \times 10^6$  and simulate  $\sigma(S_F)$  for 400 times. In this case,  $C_0$  is calculated as the average of the ratio of  $\sigma(S_F)$  and  $V_{STD}$ , i.e.,

$$C_0 = \frac{1}{400} \sum_{i=1}^{400} \frac{\sigma(S_F)}{\sqrt{V_{STD}}} = 5.26 \quad (16)$$

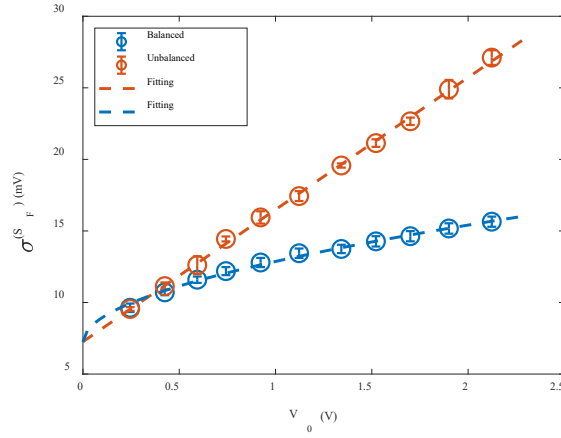


Figure 16: The orange circles show the standard deviation of the signal when monitoring the signal from one detector only, and the blue circles show the same when the signals from the two detectors are subtracted. The dashed lines show the simulations. See text for details.

In Figure 16, the orange circles show the standard deviation of the signal when the input to PD1 is blocked, and the blue circles show the same when the signals from the two detectors are subtracted. As can be seen, the noise seen by a single detector is a linear function of the light intensity. As such, this is dominated by intensity noise in excess of the shot noise. We model this intensity noise by a linear equation:

$$\sigma_{lin}(S_F) = aV_0 + b \quad (17)$$

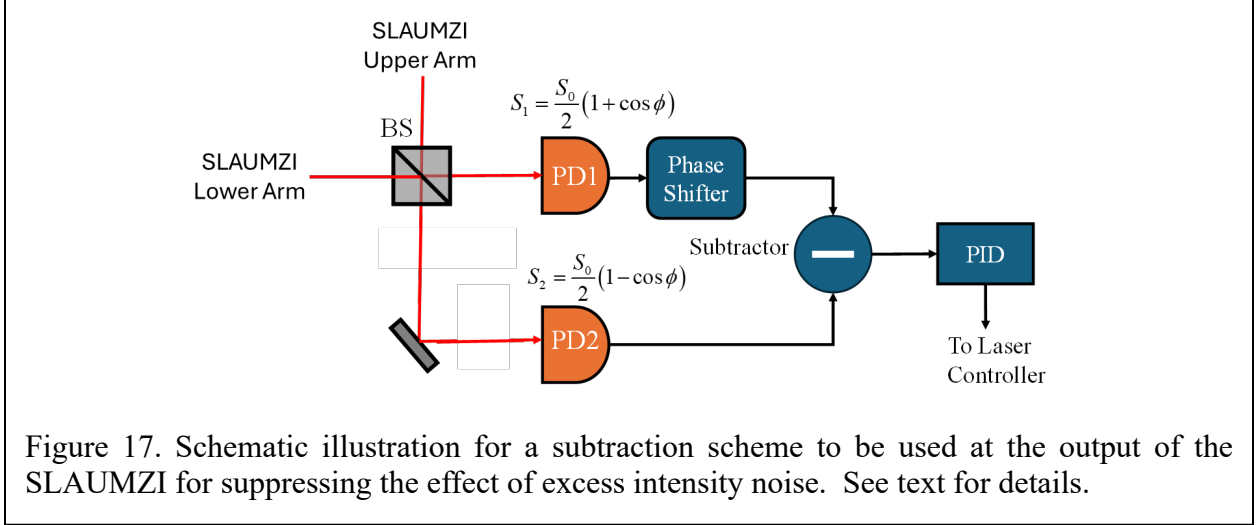
where  $a$  and  $b$  are fitting parameters, with the latter representing an offset which can be attributed to the electronic noise that is present in the absence of any light. By doing curve fitting, as shown in the dashed red line,  $a$  and  $b$  are found to be 9.23 and 7.26, respectively.

When subtraction is activated, the noise grows much more slowly as a function of intensity. Due to the imperfection of the subtraction process, and the fact that the excess linear noise may have a bandwidth that exceeds the bandwidth of the subtraction system, it is expected that there will be a small portion of intensity noise left after the subtraction. Therefore, a linear term is introduced in Eq.(15) to account for the residual intensity noise. Here we define a fitting parameter  $p$ , which is interpreted as the percentage of intensity noise left in the subtracted signal. Therefore, the fitting equation for the noise observed after subtraction can be expressed as:

$$\sigma(S_F) = C_0\sqrt{V_0} + p * a * V_{STD} + b. \quad (18)$$

Figure 16 shows the optimum fitting when  $p = 0.038$ . The fact that the standard deviation in this case is dominated by the part that grows as the square root of the intensity indicates that the subtraction technique is able to extract efficiently the shot noise by suppressing the excess noise.

If this subtraction scheme is used for the SLAUMZI apparatus, it is important to ensure that the signal that corresponds to the frequency shift does not get suppressed. As such, we propose a two-port detection technique, as illustrated in Figure 17. The BS shown here corresponds to the output BS of the SLAUMZI apparatus. Outputs from both ports of this BS are detected by using



two matched PDs. We denote the received signals at PD1 and PD2 as  $S_1$  and  $S_2$ , respectively. These can be expressed as:

$$S_1 = \frac{S}{2}(1 + \cos \phi); \quad S_2 = \frac{S}{2}(1 - \cos \phi) \quad (19)$$

where  $S$  is the peak signal and  $\phi$  is the phase difference between the two arms in the SLAUMZI. We can express the peak signal as:

$$S = \langle S \rangle + (\Delta S)_{SN} + (\Delta S)_{IN}; \quad \langle S \rangle \equiv S_0; \quad (\Delta S)_{IN} = \alpha S_0 \quad (20)$$

Here,  $S_0$  represents the mean value,  $(\Delta S)_{SN}$  represents the shot noise, and  $(\Delta S)_{IN} = \alpha S_0$  represents the intensity noise, with  $\alpha$  representing the ratio between the intensity noise and the mean signal. We assume the phase-shifter has been optimized and the bandwidth of the subtractor exceeds the bandwidth of the PDs. Under these conditions, it is reasonable to assume, based on the results reported above, that the intensity noise seen by the two PDs would be correlated. Since the shot noise seen by the two detectors would be uncorrelated, we can express the subtracted signal as:

$$\begin{aligned} S_D &= S_1 - S_2 = S_0 \cos \phi + (\Delta S_D)_{IN} + (\Delta S_D)_{SN} \\ (\Delta S_D)_{IN} &= \alpha S_0 \cos \phi \\ (\Delta S_D)_{SN} &= \sqrt{(\Delta S)_{1,SN}^2 + (\Delta S)_{2,SN}^2} \end{aligned} \quad (21)$$

We can choose the operating point of the SLAUMZI so that the phase difference  $\phi \equiv \phi_c = \pi/2$ , corresponding to the point where the derivative  $|\partial S_D / \partial \phi|$  is maximized. At  $\phi_c$ , both the mean

signals and the intensity noises seen by PD1 and PD2 cancel out, leaving only the shot noise. To determine the minimum measurable phase shift (MMPS) at this operating point, we assume for simplicity that each detector has unit quantum efficiency, and the signal is dimensionless, representing the number of photons observed during the measurement time. It then follows that, at  $\phi = \phi_c$ :

$$(\Delta S_D)_{IN} = 0; (\Delta S_D)_{SN} = \sqrt{S_0/2 + S_0/2} = \sqrt{S_0} \quad (22)$$

Therefore, the MMPS at  $\phi = \phi_c$  is:

$$\delta\phi|_{\phi=\phi_c} = \frac{(\Delta S_D)_{\phi=\phi_c}}{|\partial S_D / \partial \phi|_{\phi=\phi_c}} = \frac{\sqrt{S_0}}{S_0} = \frac{1}{\sqrt{S_0}} \quad (23)$$

which is the MMPS achievable under shot-noise limit. It should be noted that in determining the slope of the signal as a function of the phase, we take into account only the mean value of  $S_D$ .

It should be noted that in this scheme we have ignored other types of excess noise that may not be proportional to the mean intensity. If we denote such noise as  $\Delta S_{exc}$ , then the value of MMPS at  $\phi = \phi_c$  would be:

$$\delta\phi|_{\phi=\phi_c} = \frac{\sqrt{S_0 + \Delta S_{exc}^2}}{S_0} = \frac{1}{\sqrt{S_0}} \left(1 + \Delta S_{exc}^2 / S_0\right)^{1/2}; \quad \beta_{exc} \equiv \Delta S_{exc}^2 / S_0 \quad (24)$$

Thus, for  $\beta_{exc} \ll 1$ , this scheme will yield a sensitivity very close to the shot-noise limit, enabling one to reach the maximum enhancement in sensitivity due to the slow-light effect.

Note that that a similar suppression of the intensity noise can in principle be achieved by using a single detector that monitors the signal at only one of the output ports, while operating at the phase where the mean value of the signal vanishes (if the port for PD1 is used, this would occur at  $\phi = \pi$ ). In that case, both the noise and the slope of the mean signal have null values, with the ratio being  $1/\sqrt{S_0}$ , thus yielding the same value of the MMPS as what is shown in Eq. (23). However, when the excess noise that is not proportional to intensity is taken into account, the MMPS in this approach would diverge even when  $\beta_{exc} \ll 1$ .

---

[1] R. M. Howard, "White noise: A time domain basis," 2015 International Conference on Noise and Fluctuations (ICNF), Xi'an, China, 2015, pp. 1-4, doi: 10.1109/ICNF.2015.7288581.